Evaluation of Mathematical Model to Characterize the Performance of Conventional and Hybrid PV Array Topologies under Static and Dynamic Shading Patterns

Manoharan Premkumar [1], Umashankar Subramaniam [2], Thanikanti Sudhakar Babu [3], Rajvikram Madurai Elavarasan [4,*] and Lucian Mihet-Popa [5,*]

[1] Department of Electrical and Electronics Engineering, GMR Institute of Technology, Rajam, Andhra Pradesh 532127, India; premkumar.m@gmrit.edu.in

[2] Renewable Energy Laboratory, Prince Sultan University, Salahuddin, Riyadh 12435, Saudi Arabia; usubramaniam@psu.edu.sa

[3] Department of Electrical Power Engineering, University Tenaga Nasional, Kajang 43000, Selangor, Malaysia; sudhakarbabu66@gmail.com

[4] Department of Electrical and Electronics Engineering, Sri Venkateswara College of Engineering, Tamil Nadu 602117, India

[5] Faculty of Electrical Engineering, Ostfold University College, NO-1757 Halden, Norway

* Correspondence: rajvikram787@gmail.com (R.M.E.); lucian.mihet@hiof.no (L.M.-P.)

Abstract: The analysis and the assessment of interconnected photovoltaic (PV) modules under different shading conditions and various shading patterns are presented in this paper. The partial shading conditions (PSCs) due to the various factors reduce the power output of PV arrays, and its characteristics have multiple peaks due to the mismatching losses between PV panels. The principal objective of this paper is to model, analyze, simulate and evaluate the performance of PV array topologies such as series-parallel (SP), honey-comb (HC), total-cross-tied (TCT), ladder (LD) and bridge-linked (BL) under different shading patterns to produce the maximum power by reducing the mismatching losses (MLs). Along with the conventional PV array topologies, this paper also discusses the hybrid PV array topologies such as bridge-linked honey-comb (BLHC), bridge-linked total-cross-tied (BLTCT) and series-parallel total-cross-tied (SPTCT). The performance analysis of the traditional PV array topologies along with the hybrid topologies is carried out during static and dynamic shading patterns by comparing the various parameters such as the global peak (GP), local peaks (LPs), corresponding voltage and current at GP and LPs, fill factor (FF) and ML. In addition, the voltage and current equations of the HC configuration under two shading conditions are derived, which represents one of the novelties of this paper. The various parameters of the SPR-200-BLK-U PV module are used for PV modeling and simulation in MATLAB/Simulink software. Thus, the obtained results provide useful information to the researchers for healthy operation and power maximization of PV systems.

Keywords: GP; LPs; mismatching loss; partial shading; power maximization; PV array

1. Introduction

India has always been a prominent country in terms of renewable energy aspects especially solar and wind in comparison with other countries in the world [1]. There are also some significant states in India, where solar energy resource was a vital source and whose solar potential is also high [2,3].

The solar photovoltaic (PV) power generation has been attracting because of the reduction in the PV module price, government incentives and innovative commercial models. However, the solar PV power generation systems have demerits, such as low energy conversion and high installation cost. The PV module has a non-linear voltage–current (V–I) characteristic, and there must be a maximum operating point on the power–voltage (P–V) characteristic. The power output of the PV module depends on the temperature and solar insolation. To improve the efficiency of the PV system, the module should be operated at the maximum power point [4–7]. However, the effectiveness of the system is reduced by a partial shading effect on the module/array. This shading effect is due to various factors such as building, tree, cloud, dust, etc. Due to partial shading conditions (PSCs), there are many peaks on the V–I and P–V characteristics of the PV module/array, which reduces the output power of the PV system [8,9].

Out of various factors that affect the performance of the PV module, the change in solar insolation and temperature are considered as critical factors. Under uniform irradiation, the PV panel exhibits a single maximum power point (MPP). Additionally, the MPP can be tracked using conventional methods such as perturb & observation, incremental conductance algorithm, etc. [10,11]. During PSCs, the PV panels exhibit multiple local peaks (LPs) and one global peak (GP), as discussed earlier. Due to multiple LPs, the PV system misleads the conventional maximum power point tracking (MPPT) techniques. In order to track the GP, the advanced MPPT techniques are effectively used [12–20]. Due to PSCs, the panel mismatching power loss is more, and hence the efficiency and capability to generate the maximum power are reduced. These problems can be overcome by connecting bypass diodes across the panel. However, the total effects can be overcome by connecting bypass diodes across each cell. Since it is not economical, the bypass diodes are connected across the group of cells. Some of the manufacturers are providing the PV module with two or three bypass diodes. In addition to PSC, power loss is also due to other factors, such as soiling, dust, bypass diode degradation, etc. [21]. The power loss can be reduced by the different PV array configurations, MPPTs, PV system architecture and converter topologies. Out of which, the different PV array configuration is one of the optimum ways that can reduce mismatching losses under PSCs. The PV array configurations are based on different electrical interconnection between the PV panels [22–28]. The PV architecture defines different methods of connecting power converters to the PV module/array, i.e., central level inverter, string inverter and microinverter [3]. The various MPPT techniques, such as distributed MPPT, central-level MPPT, module-level MPPT and reconfigurable MPPT, are also developed to reduce the mismatching losses (MLs) [29,30]. The PV arrays are formed using different configurations such as series-parallel (SP), total-cross-tied (TCT), bridge-linked (BL), honey-comb (HC) and ladder (LD) to attain the desired output voltage and current for grid-tied systems or standalone systems. The classification of the different configurations is given in Figure 1. The panels are connected in series to make a string, and the strings are connected in parallel to each other to get the desired voltage and current in SP array configurations. In the TCT array configuration, all nodes of rows are shortened in the SP array. The node voltages of all nodes and the sum of currents at various junctions are the same. In the BL configuration, the modules are connected in the form of a bridge rectifier in which the first few panels are connected in series and parallel to each other. By combining the advantages of TCT and BL, a modified BL configuration, named HC, is formulated [31–34].
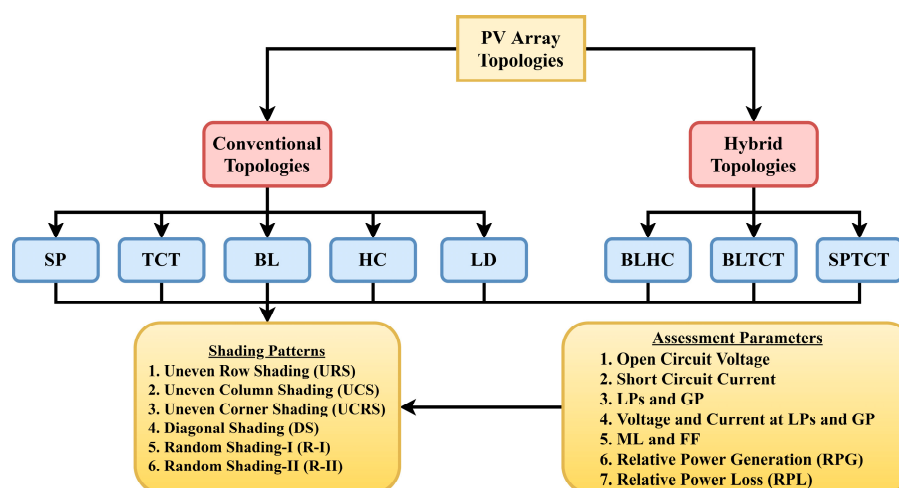
Figure 1. Different photovoltaic (PV) array topologies for the discussions.

The authors of [30,35] have discussed the ladder structure of the PV array to extract high output power during PSCs. The authors of [36,37] have discussed hybrid solar PV array topologies such as bridge-linked honey-comb (BLHC), bridge-linked total-cross-tied (BLTCT) and series-parallel total-cross-tied (SPTCT) configurations. The combination of BL and HC configuration is called BLHC, which has advantages of both BL and HC array configurations. The combination of BL and TCT configuration is called BLTCT and the combinations of SP and TCT configuration is called SPTCT configuration. These hybrid configurations are proposed by the researchers to minimize the panel mismatching losses, and these configurations are more competitive to the conventional PV array configurations. The authors of [38,39] investigated the PSC effect on the SP PV array configuration. The authors of [40] investigated the PSC effects on various PV array configurations such as SP, TCT and BL (6 × 2, 4 × 3, 2 × 6 and 3 × 4 array size). The authors of [41,42] presented a method to improve the power output during PSCs. Many studies have been conducted on the various PV array configurations under PSCs, and from each study, the superiority of the respective configuration is proved through a sequence of simulations. The researchers use a different method such as different PV array configurations, reconfigurable PV array topologies and different MPPT techniques to reduce mismatching loss, and the same can be explained briefly as follows.

(a) Comparison of different PV array configurations

The author of [43] discussed a comparison between the various array configurations such as the series (S) PV array and SP PV array under PSCs. The modeling is done with the help of MATLAB/Simulink. The author concluded that the magnitude of GP depends on the shading pattern and array configurations. A detailed comparison is made on different PV array configurations under even and uneven column and row shadings [9]. The author concluded that out of different configurations, TCT array configuration is performing better under the different shading patterns. However, the author of [44] strongly disagrees with the widely held findings that SP PV array configuration is a highly efficient configuration in extracting maximum output power from the PV array. The author of [45] reviewed and generated M-code to study and compare the effects of PSCs on different PV array configurations. According to the author, HC and TCT are more effective than the other configurations under symmetric and asymmetric PV array configurations. The author of [24] discussed the performance comparison of the different PV array configurations such as S, SP, TCT, BL and HC under PSCs. The author also discussed non-linear equation solving using the Newton–Raphson algorithm. The authors of [46] discussed various PV array configuration and suggested to employ current injection technique to diminish the effect of PSCs on the PV array. The authors of [47] presented two types of PV array configurations, such as TCT and non-symmetrical, and tested on various shaded patterns to check the effectiveness of the array configurations, and proved that non-symmetrical configurations perform better than the TCT configuration. The authors

of [48–51] discussed PV array topologies such as SP, BL, TCT and all authors claimed that TCT configuration performs better than the other configurations. The authors of [52–56] discussed a detailed procedure for modeling the PV array of any configuration, which is operating under uniform or PSCs. The authors of [57] presented an array of parallel-connected PV cells along with a low input voltage boost converter, and a wide bandwidth MPP technique to improve the output power of the PV array during PSCs and rapid shadow conditions. The model to find an optimal photovoltaic system configuration for the specified installation area that makes maximum profit over a lifetime of the PV energy plant is discussed in [58].

(b) Modern PV array configurations

The author of [59] discussed a dynamic PV array reconfiguration system for the building-integrated PV systems and large PV plants. However, the operational and running cost of the systems and system complexity is more. The author of [60] discussed a technique to produce the maximum output power under PSCs. The method is employed with TCT configurations, but the physical location of the panel is rearranged based on the SU-DO-KU puzzle. However, due to the additional wiring requirements and unsuccessful distribution of shading, this method is not preferred. Modified SU-DO-KU based reconfiguration was proposed by [61]. It uses fixed reconfiguration, and it enhances the PV output power under mutual shading patterns. It overcomes the drawbacks of the conventional SU-DO-KU based PV array reconfigurations. The authors of [62–65] presented an adaptive PV reconfiguration under PSCs and malfunctioning situations. This technique divides the PV panel into the adaptive bank and fixed panels. If the fixed PV panels are shaded, the shaded panels are connected to the unshaded panels in the adaptive bank. However, this method requires additional sensors and switches for the implementation. Recently, the authors of [66] proposed an improved SU-DO-KU technique, and the technique was tested on 9 × 9 TCT PV array configuration to generate high output power under PSCs. The authors of [67] discussed a dynamical PV array reconfiguration strategy for a grid-tied PV system, and this reconfiguration is based on a plant-oriented configuration, which improves the energy production when the operating environmental situations are different. The authors of [68] discussed an adaptive reconfiguration scheme to reduce the effect of PSCs, in which a switching matrix attaches an adaptive bank to a static portion of the PV array based on a model control algorithm that improves the output power of the PV array. The authors of [69] proposed a magic square method to increase the output power by reconfiguring the location of the panels in the TCT PV array configuration. The authors of [70] proposed a new reconfiguration technique to ensure a minimum deviation from the nominal operating voltage, which improves the power output, and the same can be tested on a 4 × 4 PV cell array. The authors [71] disperse the power loss of a partially shaded PV array by reconfiguring a BLTCT hybrid topology-based mostly on the SU-DO-KU puzzle, which is known as SU-DO-KU 's BLTCT reconfigured configuration. The authors of [72] proposed a new method to predict the connection of modules into a TCT PV array. In this approach, shaded and un-shaded modules are placed in an array in such a way that the shading effects are evenly distributed in each row, thereby increasing the power of the PV array.

(c) MPPT techniques to extract more power

The author of [13,73,74] reviewed different MPPT algorithms such as P&O and incremental conductance that are implemented on the power converters to produce more energy from the PV array by matching the input impedance of the converter to match the GP of the array. The authors of [75] presented a bidirectional DC–DC converter, which helps the renewable energy systems, especially for the solar PV system to minimize the losses in the system. The author of [76] proposed a module integrated converter with MPPT architecture to generate the highest power than the conventional string or central inverter. The converter has its own MPPT controller for the single PV module, and all the converters are connected to the common bus. The drawback is that the cost of the microconverter-based PV system is higher. The authors of [77] proposed an accelerated optimization algorithm to extract the maximum power and minimize the mismatching losses of the PV system.

The author of [78] reviewed a specific conventional and modern hybrid MPPT technique to extract the high output power from the PV modules. The study guides the researcher to select the proper MPPT technique for the PV systems. However, the researchers are confused about choosing the exact MPPT technique due to the rapid research in the field of MPPTs.

After reviewing various methods, the array configuration-based methods are useful and viable for the PV systems. Moreover, it helps the conventional/modern MPPT controllers to extract the maximum output power from the PV string/array and reduces the module MLs. However, mathematical analysis is required for the readers for a better understanding of the characteristics of array configurations under PSCs. In this paper, mathematical modeling, analysis, and simulations are carried out on the various array topologies, and performance assessment is carried out on the 4 × 4 PV array. The different PV array topologies are shown in Figure 2.
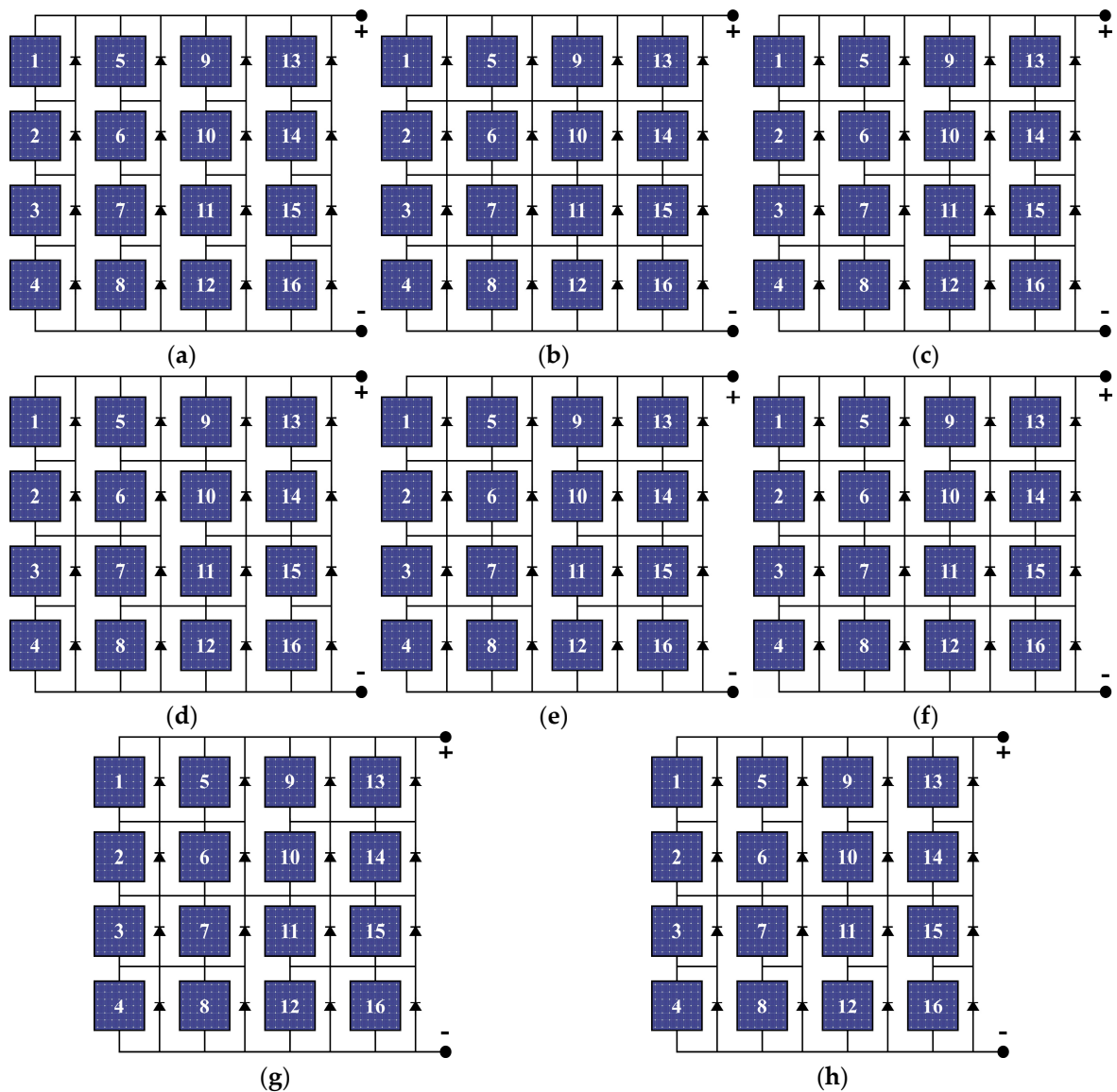
Figure 2. Solar PV array configurations: (**a**) series-parallel (SP); (**b**) total-cross-tied (TCT); (**c**) honeycomb (HC); (**d**) bridge-linked (BL); (**e**) ladder (LD); (**f**) bridge-linked honey-comb (BLHC); (**g**) bridge-linked total-cross-tied (BLTCT) and (**h**) series-parallel total-cross-tied (SPTCT).

The mathematical modeling of the HC PV array configuration is not discussed in any of the literature. Therefore, in this paper, the HC PV array configuration is elaborately discussed, and the same has been analyzed and simulated using MATLAB/Simulink. In most of the literature, the authors confirmed that TCT configuration is better in terms of ML and FF. However, this paper also

discusses various hybrid configurations (such as SPTCT, BLHC, and BLTCT) along with one new conventional LD configuration, which is more competitive to TCT. To validate and assess the performance of all the conventional topologies and hybrid topologies, an extensive simulation is carried out under various shading patterns such as an uneven row shading (URS), uneven column shading (UCS), uneven corner shading (UCRS), diagonal shading (DS) and random shadings (R-I and R-II). As presented in Figure 1, the performance assessment has been carried out in terms of open-circuit voltage (V_{oc}), short circuit current (I_{sc}), GP, LPs and its corresponding voltage and current (V_{mpp} and I_{mpp}), relative power loss (RPL), relative power generation (RPG), fill factor (FF) and the panel ML of the PV array configurations [79]. The uniqueness of this paper is that the performance assessment is carried out on various PV array configurations, including ladder structure along with the hybrid PV array configurations, which are not covered in any of the published papers so far.

The paper is organized as follows. Section 2 deals with the mathematical modeling of PV cell/module/array. Section 3 discusses the various shading patterns for the simulation. Section 4 presents the mathematical modeling of the HC PV array configuration under uneven row and column shading. Section 5 investigates the simulation results of various PV array configurations under and uniform irradiance and PSCs. Section 5 also discusses the performance of PV array configurations under dynamic shading conditions. Section 6 discusses the performance assessment of different PV array topologies, and Section 7 concludes the paper.

2. Mathematical Modeling of the PV Cell/Module/Arrays

The researchers require a reliable, feasible and flexible PV model to precisely forecast the power generated by PV cells when connected in series/parallel combinations. This section of the paper discusses a single diode PV model for the cell, and finally, it can be extended to the PV module and array. To model the PV cell/module/array, the various parameters are taken from the manufacturer's datasheet.

2.1. Modeling of a Single PV Cell Based on a Single Diode Model

The equivalent circuit of the single diode PV cell model comprises of a single current source with one anti-parallel diode, series resistance and shunt resistance [80–87]. The equivalent model of the single PV cell is shown in Figure 3.
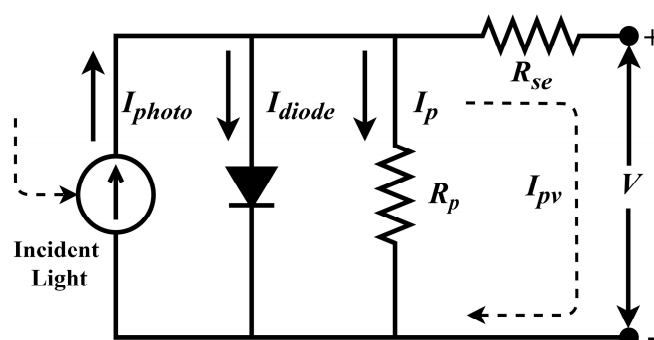

Figure 3. Equivalent PV cell model.

Apply Kirchhoff's current law for the PV cell model shown in Figure 3. The PV cell current is given in Equation (1).

$$I_{pv} = I_{photo} - I_{diode} - I_p \tag{1}$$

where I_{photo} is the photocurrent when the PV cell is subjected to incident sunlight, this current is varying linearly depends on the solar irradiance at a specific temperature. The anti-parallel diode current is I_{diode}, and it is responsible for the non-linearity of the PV cell. I_p represents the shunt resistor current, and substitute the expression for I_p and I_{diode} in Equation (1). Therefore, the cell current is derived as per Equation (2).

$$I_{pv} = I_{photo} - I_0 \left(exp\left(\frac{q(V + I_{pv}R_{se})}{akT}\right) - 1 \right) - \left(\frac{V + I_{pv}R_{se}}{R_p}\right) \tag{2}$$

where q is the electron charge, and its value is 1.602×10^{-19} C, a is the diode ideality factor, Boltzmann constant represented as $k = 1.3806503 \times 10^{-23}$ J/K, I_o is the saturation current of the diode, T represents the cell temperature and R_p and R_{se} represent the shunt and series resistance, respectively.

2.2. Modeling of a Single PV Module Based on the Single Diode Model

The PV module is made up of series-connected PV cells, and several series-connected PV cells are represented as N_{se}. For example, the SPR-200-BLK-U PV module (SunPower, CA, USA) consists of 72 PV cells, and SPR-76R-BLK-U panel (SunPower, CA, USA) consists of 24 series-connected PV cells. The output current ($I_{pv, P}$) of the PV module in terms of the output voltage (V_P) when N_{se} cells are connected in series. The total PV module current is represented in Equation (3).

$$I_{pv,P} = I_{photo} - I_0 \left(exp\left(\frac{q(V_P + I_{pv,P}R_{se})}{N_{se}akT}\right) - 1 \right) - \left(\frac{V_P + I_{pv,P}R_{se}N_{se}}{N_{se}R_p}\right) \tag{3}$$

Equation (3) can be extended to any number of series-connected PV cells, and it applies to any of the PV modules. It is not restricted to a single panel. If there are several series-connected panels (N_{mo}), and there are several series-connected PV cells in each panel (N_{ser}), then N_{se} can be rewritten as per Equation (4).

$$N_{se} = N_{mo} \times N_{ser} \tag{4}$$

2.3. Modeling of a PV Array Based on the Single Diode Model

In the PV array, the PV panels are connected in series and parallel combinations. To start with the single PV cell, several PV cells connected in series to derive the PV module and several modules connected in series to obtain PV string and several strings attached in parallel to form PV array [76]. The equivalent circuit of the PV array is shown in Figure 4. N_s represent the series-connected panels, and N_p represents the parallel-connected PV strings. The output current (I_{ar}) of PV array in terms of output voltage (V_{ar}) is presented in Equation (5).

$$I_{ar} = N_p I_{photo} - N_p I_0 \left(exp\left(\frac{q(V_{ar} + I_{ar}\frac{N_s}{N_p}R_{se})}{N_s akT}\right) - 1 \right) - \left(\frac{V_{ar} + I_{ar}R_{se}\frac{N_s}{N_p}}{\frac{N_s}{N_p}R_p}\right) \tag{5}$$

The modeling of the PV array in MATLAB/Simulink is done by using Equation (5). With the help of the following assumptions, such as $N_p I_{photo} = I'_{photo} N_p I_0 = I'_o$, $(N_s/N_p)R_{se} = R'_{se}$, and $(N_s/N_p)R_p = R'_p$ Equation (5) is modified as Equation (6).

$$I_{ar} = I'_{photo} - I'_o \left(exp\left(\frac{q(V_{ar} + I_{ar}R'_{se})}{N_s akT}\right) - 1 \right) - \left(\frac{V_{ar} + I_{ar}R'_{se}}{R'_p}\right) \tag{6}$$

With the assumptions, Equation (6) is similar to the V–I relation for a single PV cell and, it is proved that the PV array equivalent circuit is similar to the PV cell equivalent circuit. However, the variables in Figure 3 and the variables in Equation (6) have different meanings based on the above assumptions. The various parameters of the SPR-200-BLK-U PV module are used for modeling and simulating PV array topologies using MATLAB/Simulink and presented in Table 1.
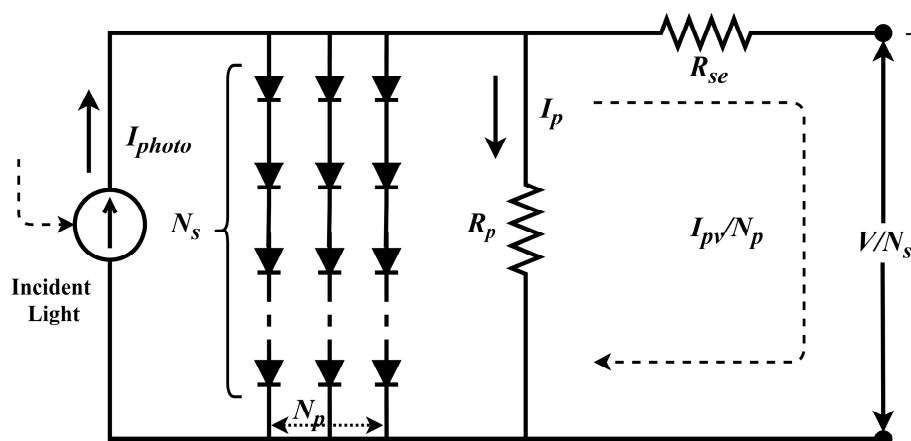
Figure 4. Equivalent circuit of the PV array.

Table 1. Parameters of SPR-200-BLK-U PV panel.

S. No.	Parameters	Symbol	Unit	Value
1	Module type	-	-	Mono-crystalline silicon
2	Number of cells	N_{se}	-	72
3	V_{oc} at standard test condition (STC)	V_{oc}	V	47.8
4	I_{sc} at STC	I_{sc}	A	5.4
5	Maximum peak current	I_{mp}	A	5
6	Maximum peak voltage	V_{mp}	V	40
7	Maximum peak power	P_{mp}	W	200
8	Temperature coefficient on I_{sc}	k_i	% / K	0.022
9	Temperature coefficient on V_{oc}	k_v	% mV / K	−0.0648
10	Series resistance	R_{se}	Ω	0.2488
11	Shunt resistance	R_p	Ω	605.48
12	Ideality factor	a	-	1.25

3. Effects and Various Shading Patterns under Partial Shading Conditions

3.1. Effects of PSC on PV Arrays

The PSCs of the conventional SP array configuration is considered as reference, and it generates panel MLs during various shading patterns. The magnitude of the MLs varies with the PV array operating point. During shading conditions, the PV module voltage is too less, and by-pass diodes short-circuit the panel to maintain the regular operation throughout the string and prevents the module from the hot spots. In most cases, the PV panels provided with two bypass diodes to reduce the power loss, as discussed in [88–92]. The panel mismatching can be noticed from the P–V characteristic, and the characteristics have multiple peaks. The P–V characteristic curve has multiple local peaks and one global peak, which misleads the MPPT algorithms. The main reasons for altering the PV panel interconnections are as follows. (i) The rise in maximum output power and (ii) multiple peak shedding. Alternative topologies have a smaller number of LPs when compared to the conventional SP configuration. Throughout the PV array, the impacts of degraded PV modules on standard operating PV panels are reduced by an extra redundancy in the circuit.

3.2. Shading Patterns

The different shading patterns under PSCs on various PV array topologies such as SP, HC, BL, TCT, LD, BLHC, BLTCT and SPTCT is described in this section of the paper. Overall, the shading patterns are grouped into two parts. Group 1, called static shading pattern, consists of four shading patterns, such as uneven row shading (URS), uneven column shading (UCS), diagonal shading (DS) and uneven corner shading pattern (UCRS). Group 2, called dynamic shading pattern, consists of two shading patterns, such as random shading-I (R-I) and random shading-II (R-II). Group 2 shading

patterns are based on several shaded panels per PV string and several PV strings randomly at any time. The solar irradiance and the shading patterns on each PV panel under PSCs are shown in Figure 5 for HC PV array configuration, and the same has been applicable for other PV array configurations.
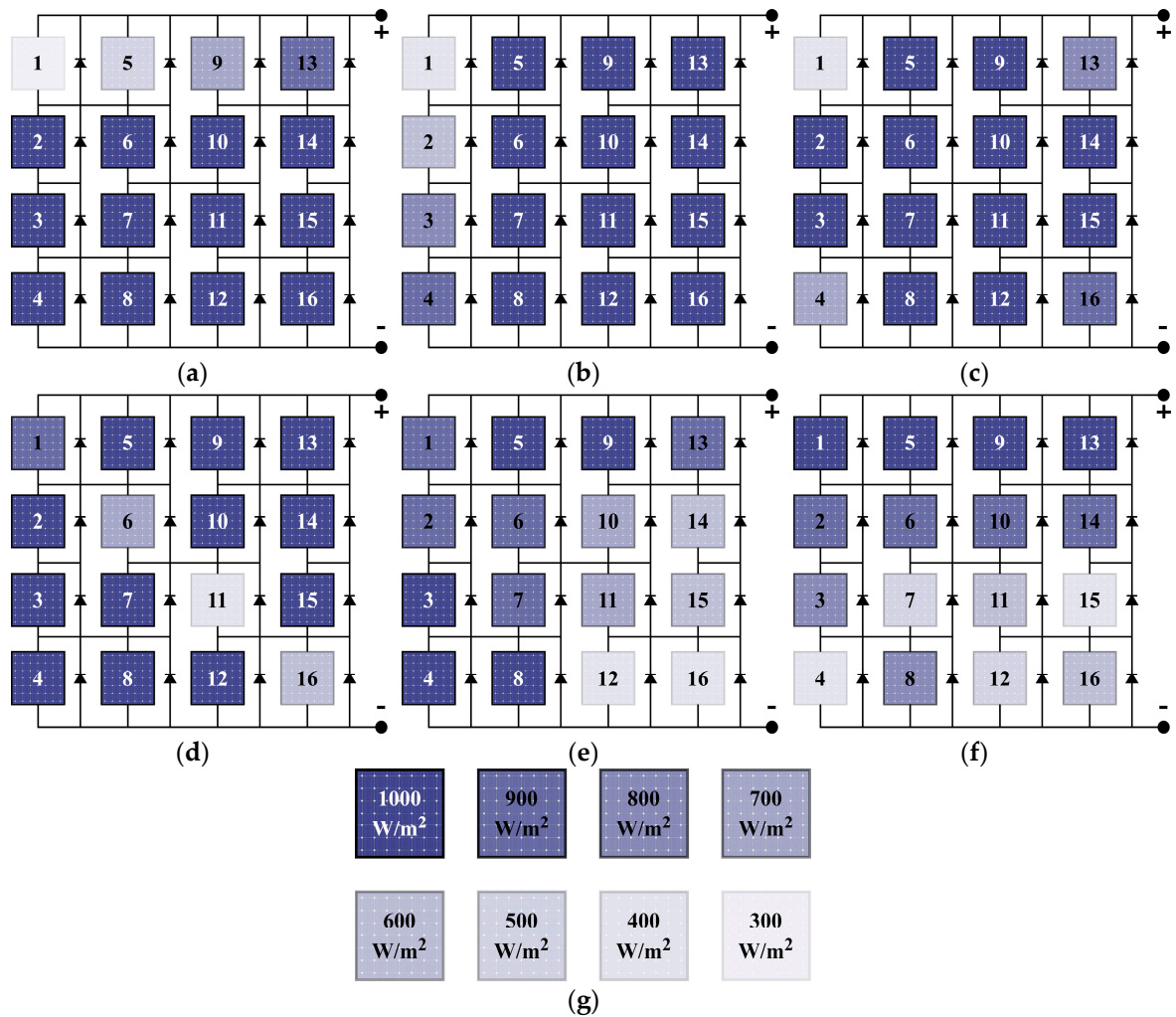

Figure 5. Sketch of different shading patterns under partial shading conditions (PSCs) on HC: (**a**) uneven column shading (UCS); (**b**) uneven row shading (URS); (**c**) uneven corner shading pattern (UCRS); (**d**) diagonal shading (DS); (**e**) random shading-I (R-I); (**f**) random shading-II (R-II) and (**g**) illustration of solar irradiance levels.

Figure 5a–f illustrates the shading patterns to be adopted in the analysis of the eight PV array configurations, as shown in Figure 2. The characteristics of PV array topologies under each shading pattern was simulated and explained in Section 5.

4. Mathematical Analysis of HC PV Array Configuration under PSCs

In HC PV array configuration, the diagonal PV modules are connected, as shown in Figure 2c. The HC PV array configuration is a modified version of the BL PV array configuration, which includes the advantages of both the TCT and BL configurations. The HC configuration is a tradeoff between TCT and BL topologies, and the main difference between the TCT and HC configuration is that the HC configuration has half of the interconnections of the TCT array configuration. However, the BL configuration has a smaller number of interconnections than the HC configurations. Moreover, all the panels in the PV array behave identically, and the output power of the PV array is similar for all the topologies when there is no module mismatch. When there is a module mismatch, one of the solar PV array topologies performance was better than the others. The performance of the HC array configuration is comparable to TCT and hybrid topologies and better than the conventional BL, LD,

S, P and SP configurations. To achieve the broad investigation of HC PV array configuration under PSCs, the mathematical analysis is required under normal operating conditions and then extended to different operating conditions. So, the most preferred 4 × 4 sized HC structure is considered as shown in Figure 6a for the mathematical analysis under normal operating conditions and analyzed at uneven row shading and uneven column shading, as shown in Figure 6b,c. The concept can be extended to all shading patterns. The module mismatch is caused by irregular solar irradiation received by each cell/module. From the equivalent circuit of the PV cell, as shown in Figure 3, the photocurrent, $I_{photo}(G)$, is directly proportional to the solar irradiance, and it is presented in Equation (7).

$$I_{photo}(G) = \frac{G}{G_o} I_{po} \tag{7}$$

where, I_{po} is the photocurrent generated at G_o (= 1000 W/m²). The V–I relationship of the cell fulfills the following function.
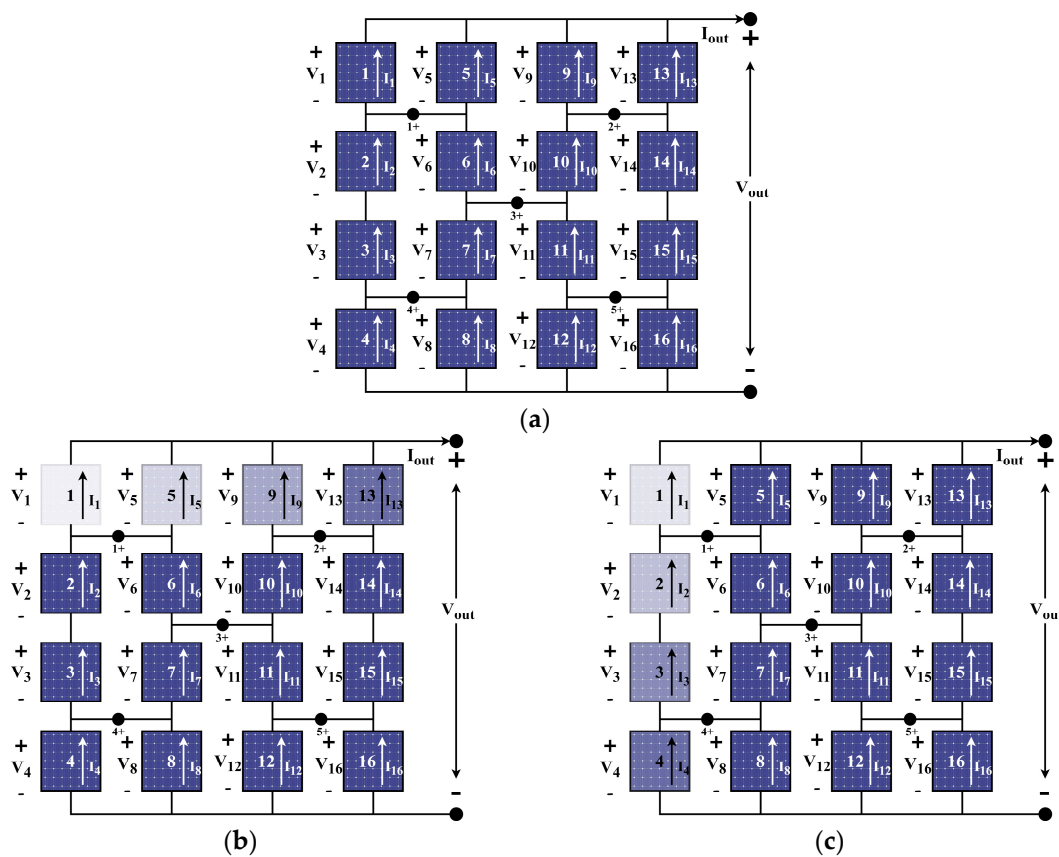

Figure 6. Mathematical analysis of HC array configuration: (**a**) normal operating condition; (**b**) uneven row shading condition and (**c**) uneven column shading condition.

$$f(I, V, G) = I_{photo}(G) + I_{diode}(V + I_{pv}R_{se}) - \frac{V + I_{pv}R_{se}}{R_p} - I = 0 \tag{8}$$

where, I_{diode} represents the diode current. When analyzing the PV array, one may start with writing the expressions governing the V–I relationships of the 16 PV modules. Apply Kirchhoff's current and voltage laws to nodes and loops to derive the equations for the respective PV array configuration. Figure 6a shows the HC array configuration, which is more accessible than the SP, TCT, BL, LD and other hybrid topologies. The V–I relationships of the 16 modules can be given by:

$$f(I_m, V_n, G_i) = 0, \qquad i = 1, 2, 3, \ldots, 16 \tag{9}$$

where, subscript '*m*' represents the current, '*n*' represents the voltage and '*i*' represents the PV module number, which are given by the below equations.

$$m = \begin{cases} 1, \text{for } i = 1 \\ 2, \text{for } i = 2, 3 \\ 3, \text{for } i = 4 \\ i - 1, \text{for } 5 \le i \le 12 \\ 12, \text{for } i = 13 \\ 13, \text{for } i = 14, 15 \\ 14, \text{for } i = 16 \end{cases} \tag{10}$$

$$n = \begin{cases} 1, \text{for } 1 \le i \le 4 \\ 5, \text{for } i = 6 \\ 6, \text{for } i = 7 \\ 7, \text{for } i = 10 \\ 8, \text{for } i = 11 \\ i, \text{for } 13 \le i \le 16 \end{cases} \tag{11}$$

It is observed that there are 12 voltages and 14 currents as variables, and hence 26 equations are required. In the HC configuration, five nodes are indicated in Figure 6a. For node numbers 1 and 4 the Kirchhoff's current law is applied, and the equations are written as:

$$I_1 + I_4 = I_2 + I_5 \tag{12}$$

$$I_3 + I_7 = I_2 + I_6 \tag{13}$$

Similarly, for the node number at 3, the equation can be written as:

$$I_6 + I_{10} = I_5 + I_9 \tag{14}$$

Similarly, for node numbers 2 and 5, the equation can be written as:

$$I_9 + I_{13} = I_{12} + I_8 \tag{15}$$

$$I_{11} + I_{14} = I_{13} + I_{10} \tag{16}$$

For each loop, the Kirchhoff's voltage law is applied, and the equations are given as,

$$V_1 = V_5; V_4 = V_8 \tag{17}$$

$$V_2 + V_3 = V_6 + V_7 \tag{18}$$

$$V_{14} + V_{15} = V_{10} + V_{11} \tag{19}$$

$$V_9 = V_{13}; V_{12} = V_{16} \tag{20}$$

$$V_6 + V_7 = V_{10} + V_{11} \tag{21}$$

Finally, apply Kirchhoff's voltage law for the loop containing the four modules in the first column, and the output voltage is given by,

$$\sum_{n=1}^{4} V_n = V_{out} \tag{22}$$

The schematic of Figure 6a contains 14 currents and 12 voltages, summing up to 26 unknown variables. Equation (9) gives 16 V–I relationship Equations, Equations (12)–(16) gives five current Equations, and Equations (17)–(21) gives five voltage equations, summing up a total of 26 equations, which is equal to the number of unknown variables. Equations (10)–(22) can be applied for the HC array configuration under normal operating conditions. This concept can be extended to different operating conditions.

Based on the above discussions and by considering Figure 6b,c, it is concluded that the sum of node currents at different nodes and the voltage of parallel modules are equal. The expressions for the node voltage, total current, and voltage of the array is given in Equations (23)–(25), respectively.

$$V_1 = V_5; V_9 = V_{13}; V_4 = V_8; V_{12} = V_{16}; V_2 + V_3 = V_6 + V_7; V_6 + V_7 = V_{10} + V_{11} \\ = V_{14} + V_{15} \tag{23}$$

$$I_{out} = I_1 + I_5 + I_9 + I_{13} \tag{24}$$

$$V_{out} = V_{13} + V_{14} + V_{15} + V_{16} = V_1 + V_2 + V_3 + V_4 \tag{25}$$

The PV modules are shaded by term α for the three-shading pattern of HC configurations, as shown in Figure 6b,c. The shading factor, α, is given in Equation (26).

$$\alpha = 1 - \frac{G}{G_o} \tag{26}$$

where G_o is the incoming solar irradiance, and G is the solar irradiance after shading. The panel currents from I_1–I_{16} are obtained from Equation (3). For unshaded PV panels, the photocurrent, I_{photo} is defined as follows.

$$I_{sc} = \frac{G_o}{1000} \times I_{photo} \tag{27}$$

where, I_{sc} is the short circuit current of the PV module, and for the shaded module, the photocurrent is defined as follows.

$$I_{sc} = \frac{(1 - \alpha)G_o}{1000} \times I_{photo} \tag{28}$$

4.1. Case-I: Uneven Row Shading

As presented in Figure 6b, the modules in the first row are shaded unevenly, and the expressions for the currents can be derived and given in Equations (29)–(33).

$$I_2 = I_3 = I_4 = I_6 = I_7 = I_8 = I_{10} = I_{11} = I_{12} = I_{14} = I_{15} = I_{16} \tag{29}$$

$$I_{16} = I_{photo} - I_0 \left(exp \left(\frac{q(V_{PU} + I_{pv,P}R_{se})}{N_{se}akT} \right) - 1 \right) - \left(\frac{V_{PU} + I_{pv,P}R_{se}N_{se}}{N_{se}R_p} \right) \tag{30}$$

$$V_{PU} = V_{2,3,4,6,7,8,10,11,12,14,15,16} \tag{31}$$

$$I_1 = I_5 = I_9 = I_{13} \\ = I_{photo} - I_{photo} \frac{\alpha G}{1000} - I_0 \left(exp \left(\frac{q(V_{PS} + I_{pv,P}R_{se})}{N_{se}akT} \right) - 1 \right) \\ - \left(\frac{V_{PS} + I_{pv,P}R_{se}N_{se}}{N_{se}R_p} \right) \tag{32}$$

$$V_{PS} = V_{1,5,9,13} \tag{33}$$

Substitute Equations (29)–(33) in Equations (24)–(25), the V–I relation can be developed as follows:

$$I_{out} = 4I_{photo} - I_{photo} \frac{\alpha G}{1000} - 4I_0 \left(exp \left(\frac{q(V_{PS} + I_{pv,P}R_{se})}{N_{se}akT} \right) - 1 \right) \\ - 4 \left(\frac{V_{PS} + I_{pv,P}R_{se}N_{se}}{N_{se}R_p} \right) \tag{34}$$

By considering Equation (25), substitute the expression for V_{PS} in Equation (34), and the expression is as follows:

$$I_{out} = 4I_{photo} - I_{photo} \frac{\alpha G}{1000} - 4I_0 \left(exp \left(\frac{q(V_{PS1} + I_{pv,P}R_{se})}{N_{se}akT} \right) - 1 \right) \\ - 4 \left(\frac{V_{PS1} + I_{pv,P}R_{se}N_{se}}{N_{se}R_p} \right) \tag{35}$$

$$V_{PS1} = V_{out} - (V_2 + V_3) - V_4 \tag{36}$$

From Equations (24)–(25), the expressions for the node voltage are given below.

$$V_4 = \frac{N_{se}aKT\left[ln\left(I_{photo} * \frac{I_{out}}{4} * \frac{I_{pv,P}R_{se}}{R_p}\right)\right] - qI_{pv,P}R_{se}}{q} \tag{37}$$

$$V_2 + V_3 = \frac{2N_{se}aKT\left[ln\left(I_{photo} * \frac{I_{out}}{4} * \frac{I_{pv,P}R_{se}}{R_p}\right)\right] - 2qI_{pv,P}R_{se}}{q} \tag{38}$$

4.2. Case-II: Uneven Column Shading

As presented in Figure 6c, the modules in the first column are shaded unevenly, and the expressions for the currents can be derived and given in Equations (39)–(46).

$$I_5 = I_6 = I_7 = I_8 = I_9 = I_{10} = I_{11} = I_{12} = I_{13} = I_{14} = I_{15} = I_{16} \tag{39}$$

$$I_{16} = I_{photo} - I_0\left(exp\left(\frac{q(V_{PU} + I_{pv,P}R_{se})}{N_{se}akT}\right) - 1\right) - \left(\frac{V_{PU} + I_{pv,P}R_{se}N_{se}}{N_{se}R_p}\right) \tag{40}$$

$$V_{PU} = V_{5,6,7,8,9,10,11,12,13,14,15,16} \tag{41}$$

$$I_1 = I_2 = I_3 = I_4 = I_{photo} - I_{photo}\frac{\alpha G}{1000} - I_0\left(exp\left(\frac{q(V_{PS}+I_{pv,P}R_{se})}{N_{se}akT}\right) - 1\right) - \\ \left(\frac{V_{PS}+I_{pv,P}R_{se}N_{se}}{N_{se}R_p}\right) \tag{42}$$

$$V_{PS} = V_{1,2,3,4} \tag{43}$$

Substitute Equations (29)–(33) in Equations (24)–(25), the V–I relation can be developed as follows:

$$I_{out} = 4I_{photo} - I_{photo}\frac{\alpha G}{1000} - 4I_0\left(exp\left(\frac{q(V_{PS} + I_{pv,P}R_{se})}{N_{se}akT}\right) - 1\right) \\ - 4\left(\frac{V_{PS} + I_{pv,P}R_{se}N_{se}}{N_{se}R_p}\right) \tag{44}$$

Substitute Equation (30) and Equation (32) in Equations (4)–(5), the relation can be developed as follows:

$$4I_{photo} - I_{photo}\frac{\alpha G}{1000} - 4I_0\left(exp\left(\frac{q(V_{5,6,7,8} + I_{pv,P}R_{se})}{N_{se}akT}\right) - 1\right) \\ - 4\left(\frac{V_{5,6,7,8} + I_{pv,P}R_{se}N_{se}}{N_{se}R_p}\right) = \\ 4I_{photo} - I_{photo}\frac{\alpha G}{1000} - 4I_0\left(exp\left(\frac{q(V_{9,10,11,12} + I_{pv,P}R_{se})}{N_{se}akT}\right) - 1\right) \\ - 4\left(\frac{V_{9,10,11,12} + I_{pv,P}R_{se}N_{se}}{N_{se}R_p}\right) = \\ 4I_{photo} - I_{photo}\frac{\alpha G}{1000} - 4I_0\left(exp\left(\frac{q(V_{13,14,15,16} + I_{pv,P}R_{se})}{N_{se}akT}\right) - 1\right) \\ - 4\left(\frac{V_{13,14,15,16} + I_{pv,P}R_{se}N_{se}}{N_{se}R_p}\right) \tag{45}$$

The output voltage of the array is obtained from Equation (42), Equation (25), and it can be expressed as follows:

$$V_{out} = 4V_5 \tag{46}$$

By using Equation (46) and Equation (25), the output current of the array for the case-II can be developed as follows:

$$I_{out} = 4I_{photo} - I_{photo}\frac{\alpha G}{1000} - 4I_0\left(exp\left(\frac{q\left(\frac{V_{out}}{4} + I_{pv,P}R_{se}\right)}{N_{se}akT}\right) - 1\right)$$
$$- 4\left(\frac{\left(\frac{V_{out}}{4}\right) + I_{pv,P}R_{se}N_{se}}{N_{se}R_p}\right) \tag{47}$$

4.3. Mathematical Analysis during Two Shading Cases

In Sections 4.1 and 4.2, the mathematical modeling of HC PV array configuration was discussed. The study of numerical analysis was discussed in this subsection. The investigation was as follows.

- By examining case-1, it was concluded that (i) during the shaded situations, compared to the unshaded case, the value of I_{sc} did not change, i.e., the current was almost constant, (ii) due to the ln relation in Equation (35), I–V characteristics of the HC PV array had two peaks. The point at which the I–V characteristics changed (I_n) its path could be given by $4I_{photo} - I_{photo} \times (\alpha G/1000)$.

- By examining case-2, it was concluded that (i) during the shaded situations, the I_{sc} was changed compared to unshaded condition (i.e., I_{sc} was equal to $4I_{photo} - I_{photo} \times (\alpha G/1000)$, (ii) I–V characteristics of the HC PV array had three peaks, and it did not change its directions.

I_n is the current at which the I–V characteristics change its path due to the shading. Reaching this current (I_n) causes I–V characteristics to produce a new peak, and the breaking point current depends on the shading factor (α). The results of the mathematical analysis are presented in Table 2, and these values are obtained for G_o = 1000 W/m².

Table 2. Results of mathematical analysis.

Test Cases	I_{sc} (A)	I_n (A)	Number of Peaks
Case-I	$4I_{photo}$	$4I_{photo} - 4\alpha I_{photo}$	2 (1 GP + 1 LP)
Case-II	$4I_{photo} - 4\alpha I_{photo}$	–	3 (1 GP + 2 LPs)

5. Simulation Results and Discussions

This section of the paper discussed the simulation of various 4 × 4 PV array topologies such as SP, HC, BL, TCT, LD, BLHC, BLTCT and SPTCT configurations. The MATLAB/Simulink software was used to compare various PV array configurations in terms of maximum output power under PSCs. For the simulation, 16 PV modules were used, and each PV module consisted of series-connected 72 PV cells. Each PV module was protected by the bypass diode, which was connected in anti-parallel with the module. Blocking diodes were connected to block the reverse flow of current. Assuming that the PV modules were operated at 25 °C temperature with different irradiance conditions, as presented in Figure 5.

5.1. SP PV Array Configuration

In the SP array configuration, four PV modules were connected in series to form a PV string to get the required output voltage, and then the strings (four PV strings) were connected in parallel to form the PV array getting the desired output current. This SP array configuration is commonly employed due to its economical operation and ease of connection. The array output current is the sum of individual PV string current in an array, and the array output voltage is the sum of the individual module voltage in a string. Along with bypass diode, the blocking diode was connected with the individual PV string to protect the string from the short circuit during PSCs. Under PSCs, the blocking diodes stop the backflow of the current into other string due to the voltage difference between the PV strings. In standalone systems, the blocking diodes block the reverse current from

the battery storage unit to PV array at night time or under partial shading condition. The simulation results of PV array output characteristics such as I–V and P–V under the different shading patterns are presented in Figure 7. Due to the series connection in a string, the ML was more but less than the series and parallel PV array configurations.
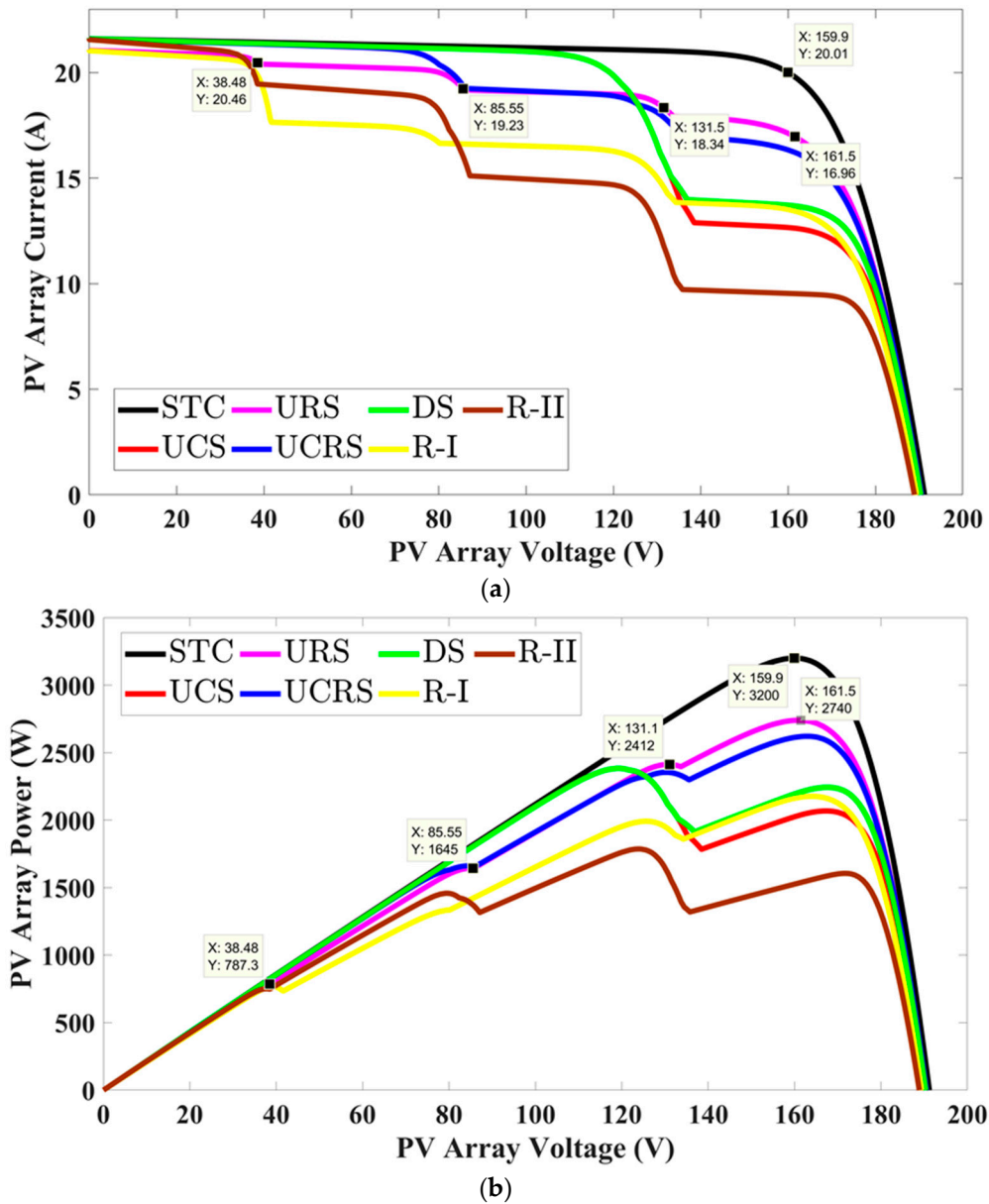
Figure 7. Output characteristics of the SP PV array configuration: (**a**) current–voltage (I–V) characteristic and (**b**) power–voltage (P–V) characteristic.

5.2. TCT PV Array Configuration

This PV configuration can overcome the drawbacks of the SP PV array configuration. In this TCT configuration, first, all the PV modules in a row were connected in parallel, and then all the rows were series-connected. In this TCT PV array configuration, the voltage across each module in a row was equal to the V_{oc} of the individual PV panel, and the PV array or required output voltage was equal to the sum of row voltages. The output current of the array is the sum of current produced from the PV panels in a row. The TCT PV array configuration utilizes a higher number of electrical wiring than the other PV array configurations. The higher number of electrical wiring made the system complex, increased the cost of the system and produced high power losses. The simulation results of

TCT PV array output characteristics such as I–V and P–V under the different shading patterns are depicted in Figure 8.

Figure 8. Output characteristics of the TCT PV array configuration: (**a**) I–V characteristic and (**b**) P–V characteristic.

5.3. BL PV Array Configuration

If a few cells in the PV module or a few PV modules in an array are subjected to PSCs, the output voltage of the whole system is reduced drastically. The SP PV array configuration consists of more series-connected modules in a string, and hence, the PV system produces more ML. To reduce the power losses in SP and S configurations, all the panels are connected in the bridge rectifier structure, as shown in Figure 2d, and this structure generally referred to as BL PV array configuration. The BL configuration consists of a more series connection than the TCT configuration and less than the S and SP configurations. So, the ML is higher than the TCT and lower than the S and SP configurations. From the structure, it can be seen that two modules in a bridge are connected in series and then connected in parallel. All the bridge structures are tied to get the required output voltage and output current. The simulation results of BL PV array characteristics such as I–V and P–V under the different shading patterns are presented in Figure 9.

(a)

(b)

Figure 9. Output characteristics of the BL PV array configuration: (**a**) I–V characteristic and (**b**) P–V characteristic.

5.4. HC PV Array Configuration

The drawbacks of the S, P, SP, BL and LD configurations can be overcome by considering HC PV array configuration. In this HC PV array configuration, the PV modules are a connected like hexagon of the honeycomb structure. The HC PV array configuration consists of a high number of series-connected PV modules than the TCT and BL and less than the S and SP PV array configuration. Therefore, the ML of HC PV array configuration was higher than the TCT, BLHC and BLTCT PV array configurations and less than the SPTCT, BL, SP and S PV array configurations. The simulation results of HC PV array output characteristics such as I–V and P–V under the different shading patterns are presented in Figure 10.
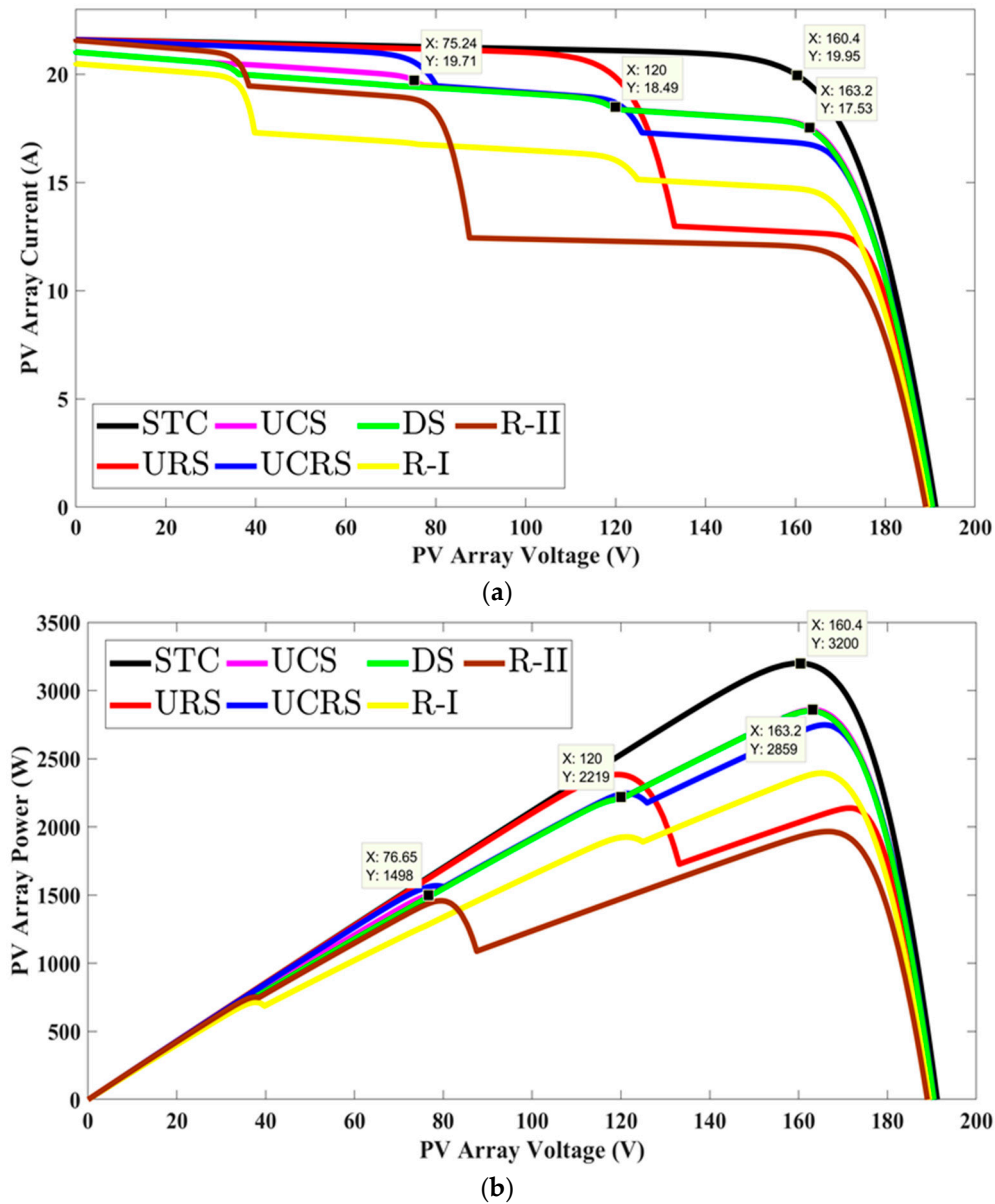
(**a**)

(**b**)

Figure 10. Output characteristics of the HC PV array configuration: (**a**) I–V characteristic and (**b**) P–V characteristic.

5.5. LD PV Array Configuration

This LD PV configuration can overcome the drawbacks of the BL and SP PV array configuration. In this LD configuration, the PV modules in a row of the first two columns were connected in parallel, and then the rows were series-connected. The structure of the LD configuration looks like a ladder. In LD PV array configuration, the voltage across each module in a row is equal to the V_{oc} of the individual PV panel. The output current of the array is the sum of current produced from the PV panels in a row. The structure of the LD is not having any series connected panels; however, the rows are connected in series. So, the ML is less than the BL, and SP and higher than the TCT, HC and other hybrid configurations. The simulation results of LD PV array output characteristics such as I–V and P–V under the different shading patterns are presented in Figure 11.
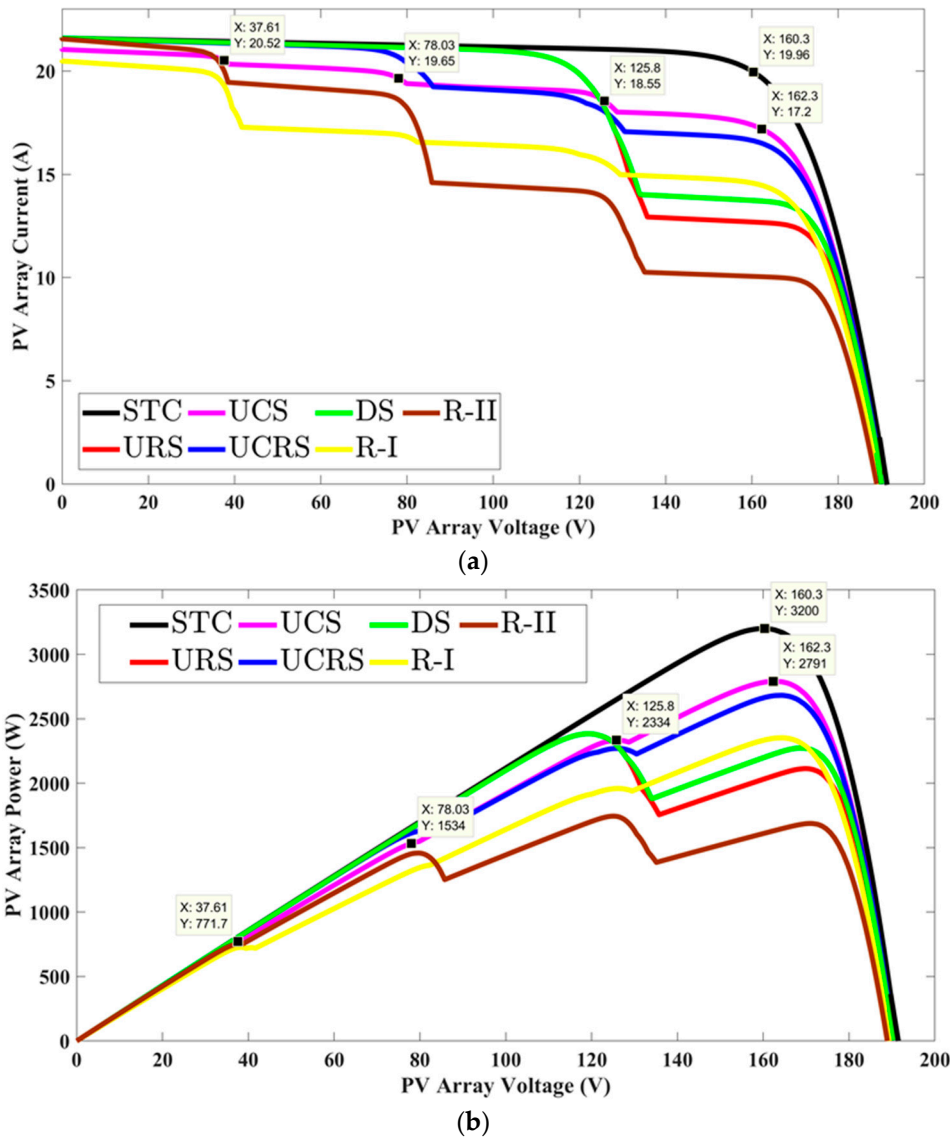
Figure 11. Output characteristics of the LD PV array configuration: (**a**) I–V characteristic and (**b**) P–V characteristic.

5.6. BLHC PV Array Configuration

This BLHC PV configuration can overcome the drawbacks of the BL, HC, LD and SP PV array configuration. In BLHC configuration, the PV modules were connected as similar to the TCT configuration except for the first-row modules. The BLHC configuration can overcome the drawback of the conventional BL and HC configurations, i.e., a smaller number of series-connected panels. The PV modules are tied together to get the desired output voltage. The number of series-connected PV modules is less than the HC, LD, BL and SP configurations. So, the ML is very less than the HC, BL, LD, SP, BLTCT, SPTCT and slightly higher than the TCT configuration. The simulation results of BLHC PV array output characteristics such as I–V and P–V under the different shading patterns are presented in Figure 12.
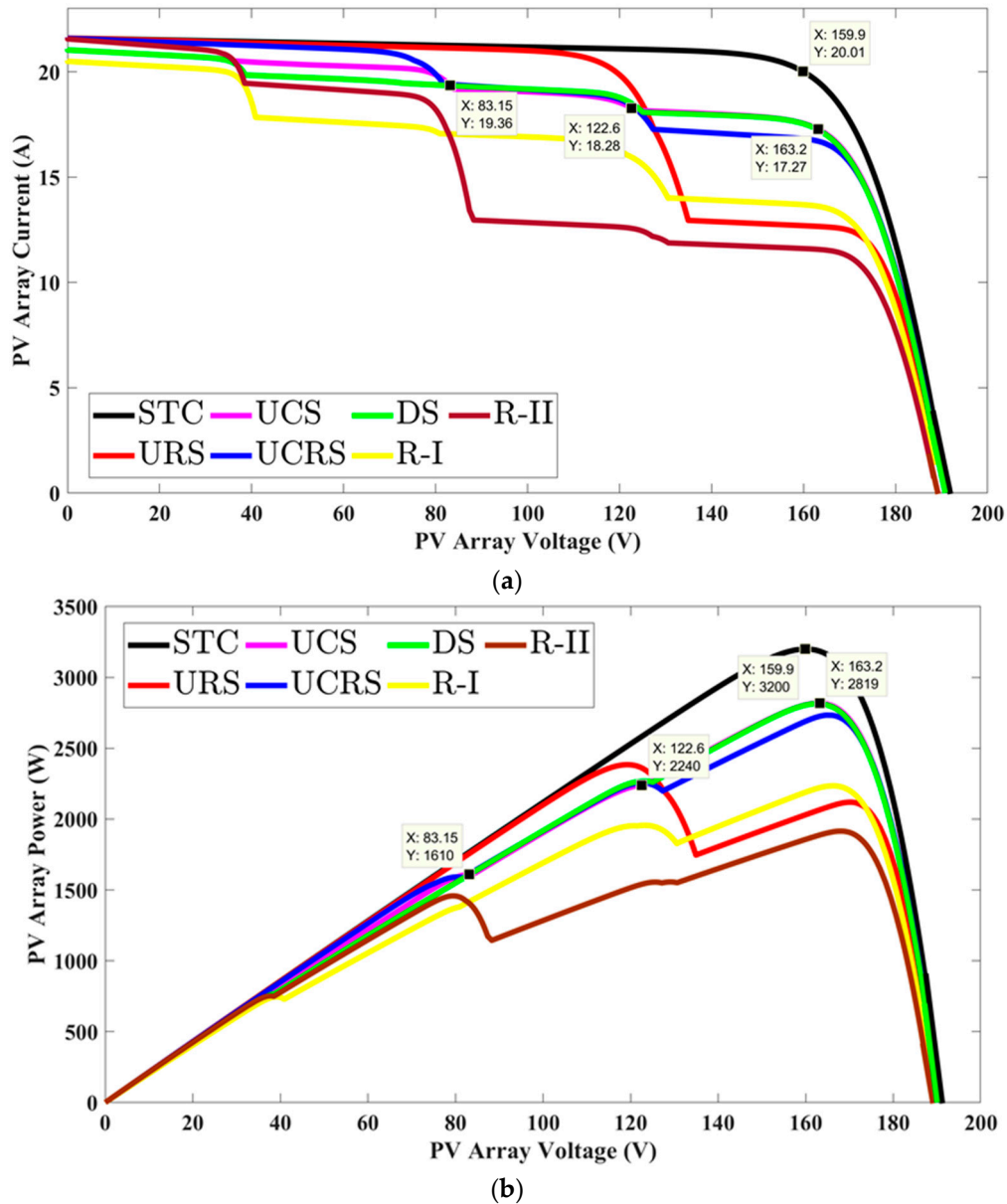
(**a**)

(**b**)

Figure 12. Output characteristics of the BLHC PV array configuration: (**a**) I–V characteristic and (**b**) P–V characteristic.

5.7. BLTCT PV Array Configuration

This BLTCT PV configuration can overcome the drawbacks of the conventional array configurations except for the TCT configuration. In the BLTCT configuration, the PV modules were connected in a similar fashion as the BL configuration except for the middle row modules in which the modules were tightly tied. The BLTCT configuration can overcome the drawback of the conventional BL and TCT configurations, i.e., a smaller number of the series-connected panels, and a smaller number of electrical wirings. The number of series-connected PV modules was less than the HC, LD, BL and SP configurations, but higher than the TCT and BLHC configurations. So, the ML was lesser than the HC, BL, LD, SP and SPTCT, and higher than the BLHC and TCT configurations. The simulation results of BLTCT PV array output characteristics such as I–V and P–V under the different shading patterns are presented in Figure 13.
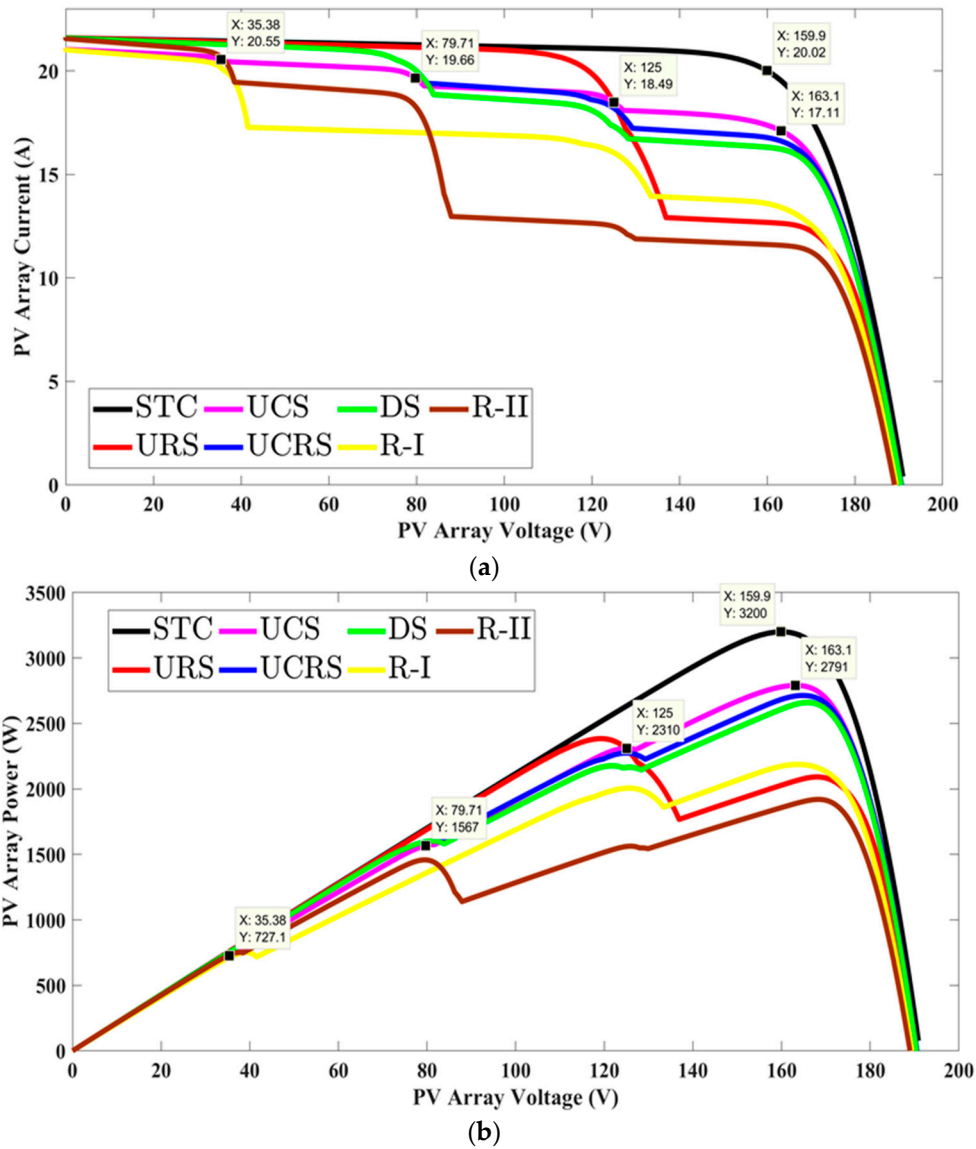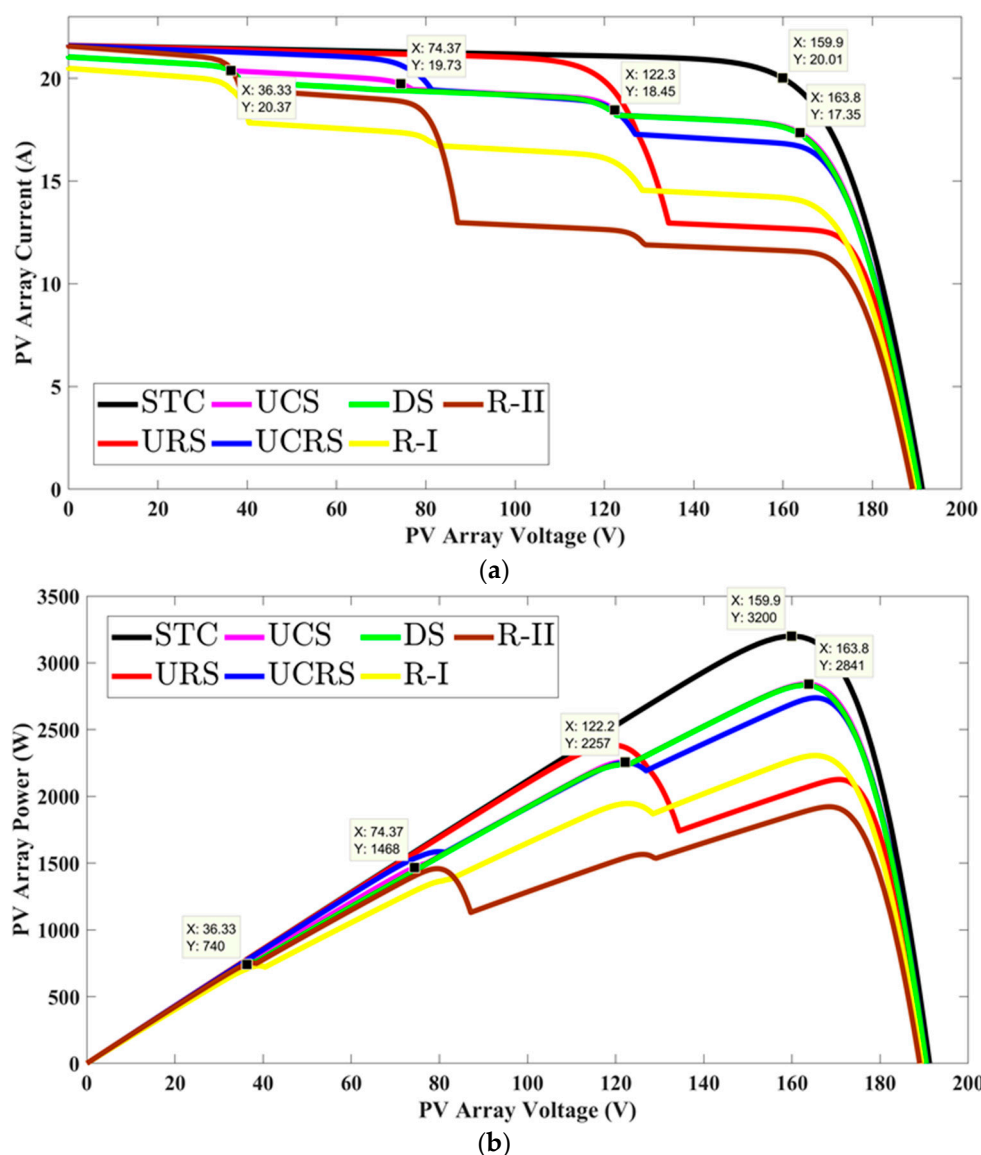
Figure 13. Output characteristics of the BLTCT PV array configuration: (**a**) I–V characteristic and (**b**) P–V characteristic.

5.8. SPTCT PV Array Configuration

The SPTCT PV configuration can overcome the drawbacks of the conventional array configurations except for the HC and TCT configurations. In SPTCT configuration, the PV modules were connected in a similar fashion as the SP configuration except for the middle row modules in which the modules were tightly tied. The SPTCT array configuration had a higher number of series-connected modules as similar to the SP configuration, but less than the SP configuration combined with the benefits of TCT configuration. The SPTCT configuration can overcome the drawback of the conventional SP and TCT configurations, i.e., a smaller number of series-connected panels, and a smaller number of electrical wirings. The number of series-connected PV modules is less than the SP configurations but higher than the other configurations. So, the ML is lesser than the BL, LD and SP, and higher than the HC, BLHC, BLTCT and TCT configurations. The simulation results of SPTCT PV array output characteristics such as I–V and P–V under the different shading patterns are presented in Figure 14.
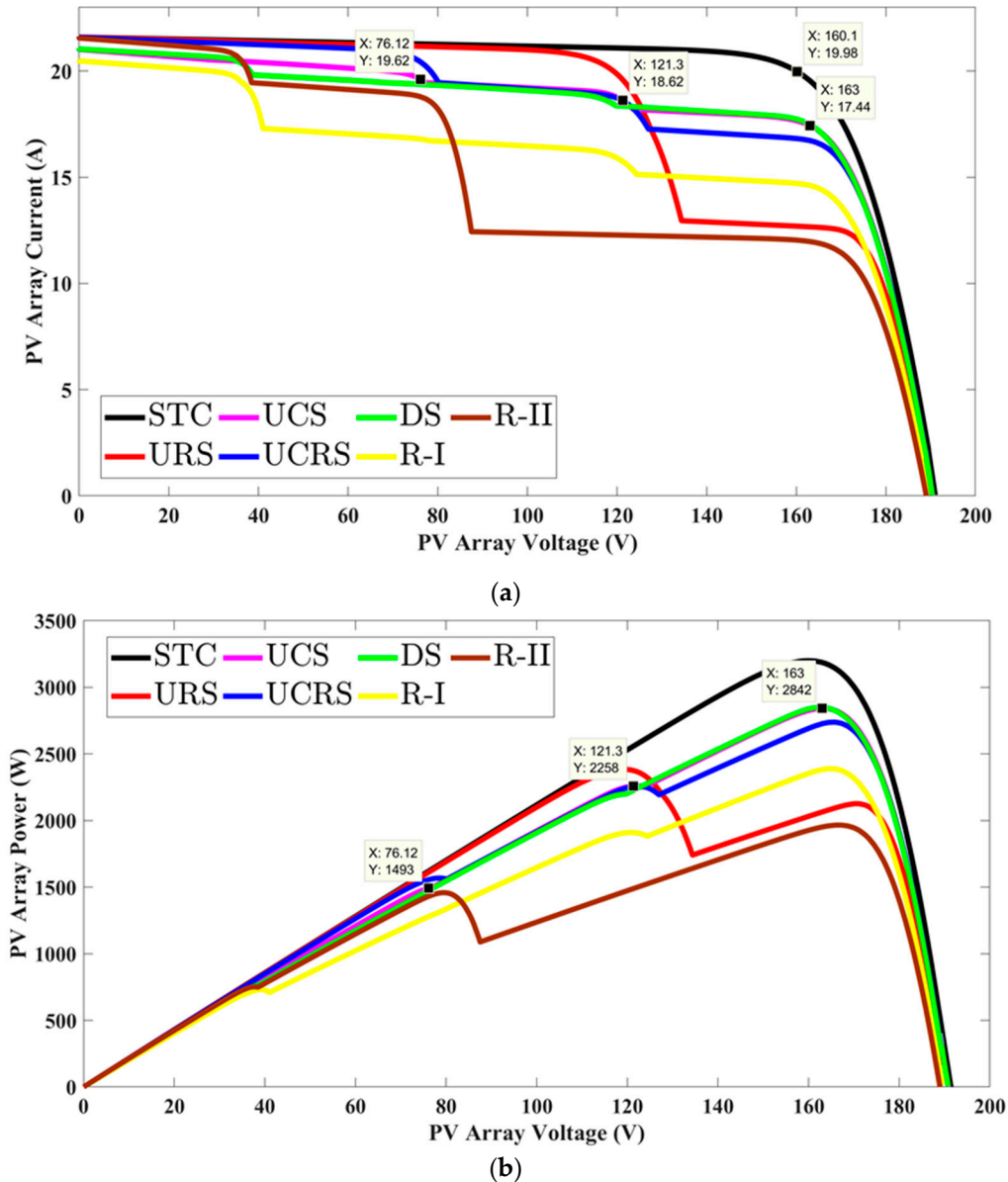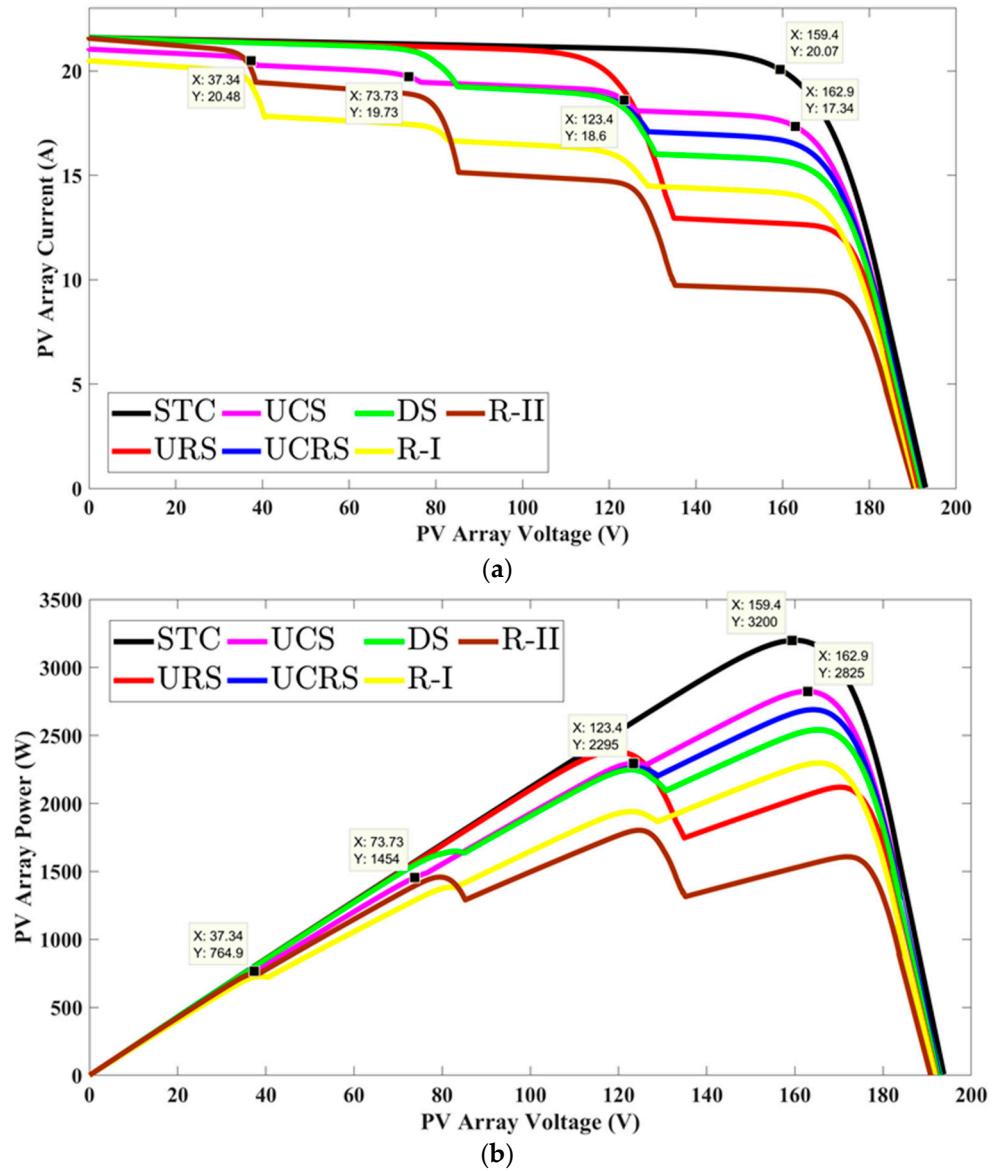
(**a**)

(**b**)

Figure 14. Output characteristics of the SPTCT PV array configuration: (**a**) I–V characteristic and (**b**) P–V characteristic.

The expressions for output array output voltage, array output current and array output power of various PV array configurations in terms of module/string voltage/current are listed in Table 3.

Table 3. PV array output voltage, current and power of different PV configurations.

Configurations	Array Output Voltage (V)	Array Output Current (A)	Array Output Power (W)
SP	$V_{out} = \sum_{i=1}^{4} V_i = 4V_i$ i = individual module voltage	$I_{out} = I_{j1} + I_{j5} + I_{j9} + I_{j13} = 4I_j$ j = individual string current	$P_o = 16 \times V_i \times I_j$
TCT	$V_{out} = V_{t1} + V_{t2} + V_{t3} + V_{t4}$ t = individual row voltage	$I_{out} = I_{t1} + I_{t5} + I_{t9} + I_{t13} = 4I_t$ j = individual string current	$P_o = 16 \times V_t \times I_t$
BL	$V_{out} = \sum_{i=1}^{4} V_i = 4V_i$ i = row of the PV array	$I_{out} = I_1 + I_5 + I_9 + I_{13} = 4I_j$ j = column of the PV array	$P_o = 16 \times V_i \times I_j$
HC	$V_{out} = \sum_{i=1}^{4} V_i = 4V_i$ i = row of the PV array	$I_{out} = I_1 + I_5 + I_9 + I_{13} = 4I_j$ j = column of the PV array	$P_o = 16 \times V_i \times I_j$
LD	$V_{out} = \sum_{i=1}^{4} V_i = 4V_i$ i = row of the PV array	$I_{out} = I_1 + I_5 + I_9 + I_{13} = 4I_j$ j = column of the PV array	$P_o = 16 \times V_i \times I_j$
BLHC	$V_{out} = \sum_{i=1}^{4} V_i = 4V_i$ i = row of the PV array	$I_{out} = I_1 + I_5 + I_9 + I_{13} = 4I_j$ j = column of the PV array	$P_o = 16 \times V_i \times I_j$
BLTCT	$V_{out} = \sum_{i=1}^{4} V_i = 4V_i$ i = row of the PV array	$I_{out} = I_1 + I_5 + I_9 + I_{13} = 4I_j$ j = column of the PV array	$P_o = 16 \times V_i \times I_j$
SPTCT	$V_{out} = \sum_{i=1}^{4} V_i = 4V_i$ i = row of the PV array	$I_{out} = I_1 + I_5 + I_9 + I_{13} = 4I_j$ j = column of the PV array	$P_o = 16 \times V_i \times I_j$

6. Performance Evaluation of Various PV Array Configurations under PSCs

This section of the paper discussed the various comparisons of evaluation parameters of different PV array topologies such as SP, TCT, BL, HC, LD, BLHC, BLTCT and the SPTCT configuration under the operating conditions such as uniform irradiance and PSCs to choose the excellent array configuration that delivers high performance. The assessment was carried out by calculating the theoretical power generations under different operating conditions, the number of LPs, fill factor (FF) and mismatching loss. The *ML* is represented as *ΔP_L*, and it was calculated as a percentage. The expression for *ΔP_L* in a percentage is given in Equation (48). The theoretical power generation was calculated as per Equation (49).

$$ML, \Delta P_L = \frac{P_{mp} - P_{PSC}}{P_{mp}} \times 100 \tag{48}$$

where, the maximum power generation under the uniform irradiance condition is represented by *P_mp*, and the power generation at certain PSC is represented by *P_PSC*. *P_PSC* can be calculated by multiplying *V_mp* and *I_mp* of GP at the respective PSC. The theoretical power generation in watts can be calculated by using Equation (49) in which *G* is solar irradiance under PSC of the individual module, *G_o* is solar irradiance under uniform irradiance and *i* is the total number of PV modules.

$$P_{the} = \sum_{i=1}^{i=16} \left(\frac{G}{G_o} \times P_{mp,i} \right) \tag{49}$$

Theoretical power generation (*P_the*) can be useful for calculating the relative power loss of the respective PV array configuration. The relative power loss (*RPL*) in watts of the solar PV array can be calculated by using Equation (50). The relative power gained (*RPG*) in percentage concerning the maximum output power of SP PV array can be calculated by using Equation (51).

$$RPL = P_{the} - P_{mp} \text{ (at GP)} \tag{50}$$

$$RPG = \frac{P_{mp,i} - P_{mp,SP}}{P_{mp,SP}} \times 100 \tag{51}$$

where the term '*i*' represent the various PV array topologies such as TCT, BL, HC, LD, BLHC, BLTCT and SPTCT, and $P_{mp,SP}$ represents the PV array output power of SP configuration. Another vital assessment parameter of the solar PV system is FF. If FF is near unity, then the performance of the solar PV system is higher. The FF can be calculated by using Equation (52).

$$FF = \frac{(V_{mp} * I_{mp}) \text{ at respective PSC}}{V_{oc} * I_{sc}} \times 100 \tag{52}$$

At first, the performance assessment of the solar PV topologies could be carried out, and then, the same was extended to other shading patterns, as shown in Figure 5. For all the assessment, the temperature was kept constant at 25 °C.

6.1. Standard Test Conditions (STCs)

In general, the standard test condition (STC) of the PV module is given by the manufacturer. The temperature at STC was 25 °C, and the solar irradiance at STC was 1000 W/m². From the simulation results, as shown in Figures 7–12, various configurations such as SP, TCT, BL, HC, LD, BLHC, BLTCT and SPTCT produced the maximum array output power of 3200 W with single LP, which is referred to as GP. The voltages and currents at OC, SC, GP and LPs are listed in Table 4 for STCs. During STCs, all the topologies produce almost the same voltage and current at GP. The ML was nearly zero, and FF was roughly equal to 77.3% for all the topologies.

Table 4. Assessment parameters of PV array configurations under the standard test condition (STC).

Configurations	V_{oc} (V)	I_{sc} (A)	GP Parameters			LP Parameters	No. of LPs	ML (%)	FF (%)
			V_{mp} (V)	I_{mp} (A)	P_{mp} (W)	$V_{mp}; I_{mp}; P_{mp}$			
SP	191.4	21.64	159.9	20.01	3200	-	-	0.031	77.32
TCT	191.2	21.62	160.4	19.98	3200	-	-	0.031	77.52
BL	191.4	21.64	160.3	19.96	3200	-	-	0.031	77.25
HC	191.2	21.64	159.9	20.01	3200	-	-	0.031	77.33
LD	191.2	21.64	159.9	20.02	3200	-	-	0.031	77.37
BLHC	191.2	21.64	160.1	19.98	3200	-	-	0.031	77.31
BLTCT	191.2	21.64	159.9	20.01	3200	-	-	0.031	77.33
SPTCT	191.2	21.64	159.4	20.07	3200	-	-	0.031	77.32

6.2. URS Pattern

For this assessment, the solar irradiance of the first-row modules is changed as per Figure 5a. The various performance parameters are listed in Table 5 for all array configurations. Under the URS pattern, all the configurations exhibited single LP and one GP. All the configurations found GP at 2384 W. The ML of all the configurations was almost equal to 25.5% with the FF varying between 57.89 and 58.08%. From the simulation results and the above discussions, it can be observed that BLHC was the better option in terms of FF, and TCT was the better option in terms of ML. However, the performance of both BLHC and TCT configurations were similar. Therefore, the researcher could select a better configuration based on the electrical wiring connections.

Table 5. Assessment parameters of PV array configurations under the URS pattern.

Configurations	V_{oc} (V)	I_{sc} (A)	GP Parameters			LP Parameters	No. of LPs	ML (%)	FF (%)
			V_{mp} (V)	I_{mp} (A)	P_{mp} (W)	V_{mp}; I_{mp}; P_{mp}			
SP	190.2	21.64	119.5	19.94	2384	167.9;12.31;2068	1	25.50	57.89
TCT	190.3	21.59	119.3	19.98	2384	171.7;12.45;2138	1	25.50	57.91
BL	190.2	21.64	119.5	19.95	2384	169.6;12.46;2113	1	25.50	57.92
HC	190.2	21.64	119.4	19.97	2384	169.7;12.48;2119	1	25.50	57.93
LD	190.2	21.63	118.8	20.06	2384	167.8;12.47;2092	1	25.50	57.93
BLHC	190.2	21.59	119.3	19.99	2384	170.7; 12.46; 2126	1	25.50	58.08
BLTCT	190.2	21.62	119.2	20.01	2384	170.4;12.48;2126	1	25.50	58.00
SPTCT	190.2	21.63	119.2	20.01	2384	170.2;12.45;2120	1	25.50	57.98

6.3. UCS Pattern

For this assessment, the solar irradiance of the first column modules was changed as per Figure 5b. The various performance parameters are listed in Table 6 for all array configurations. Under UCS pattern, the TCT produced two LPs at 2219 W; 1483 W and single GP at 163.2 V; 17.53 A; 2859 W. The ML was equal to 10.65% with FF equal to 71.48%, which was highest among all the array topologies. In addition, the configurations such as HC and BLHC also exhibited two LPs, the FF of both the configurations were greater than 70%, and MLs of both configurations were 1% higher than the TCT configuration. All the hybrid configurations had better values of FF and comparable values of % MLs but introduced three LPs, which misled the MPPT algorithms. Therefore, in all the aspects, the configurations such as TCT and BLHC exhibited better performance during the UCS pattern.

Table 6. Assessment parameters of PV array configurations under UCS pattern.

Configurations	V_{oc} (V)	I_{sc} (A)	GP Parameters			LP Parameters	No. of LPs	ML (%)	FF (%)
			V_{mp} (V)	I_{mp} (A)	P_{mp} (W)	V_{mp}; I_{mp}; P_{mp}			
SP	190.5	21.05	161.5	16.96	2740	131.1; 18.40; 2412 85.55; 19.23; 1645 38.48; 20.46; 787.3	3	14.37	68.30
TCT	190.5	21.01	163.2	17.53	2859	120; 18.49; 2219 75.24; 19.68; 1483	2	10.65	71.48
BL	190.5	21.09	162.3	17.02	2791	125.8; 18.55; 2334 78.03; 1534; 19.65 37.61; 20.52; 771.2	3	12.78	68.76
HC	190.5	21.08	163.2	17.27	2819	122.6; 18.28; 2240 83.15; 19.36; 1610	2	11.91	70.19
LD	190.5	21.09	163.1	17.11	2791	125; 18.49; 2310 79.71; 19.66; 1567 35.38; 20.55; 727.1	3	12.78	69.46
BLHC	190.5	21.08	163	17.44	2842	121.3; 18.62; 2258 76.12; 19.62; 1493	2	11.19	70.79
BLTCT	190.5	21.08	163.8	17.35	2841	122.3; 18.45; 2257 74.37; 19.73; 1468 36.33; 20.36; 740	3	11.22	70.77
SPTCT	190.5	21.05	162.9	17.34	2825	123.4; 18.59; 2295 73.73; 19.72; 1454 37.34; 20.48; 764.9	3	11.72	70.44

6.4. UCRS Pattern

For this assessment, the solar irradiance of the four corner modules were changed as per Figure 5c. The various performance parameters are listed in Table 7 for all array configurations. All the topologies produced two LPs and a single GP. Under the UCRS pattern, the TCT produced LPs at 1568 W; 2246 W and single GP at 165.7 V; 16.75 A; 2748 W. The ML was equal to 14.13% with FF equal

to 67.48%, which was highest among all the array topologies. The hybrid BLHC and BLTCT array configuration exhibited LPs at 1568 W; 2259 W, and 2253 W; 1585 W, respectively, and single GP at 2738 W with 14.44% ML and 66.40% FF. The maximum power generation was just 10 W less than the TCT configuration but it was better than the SP, BL, LD and SPTCT configurations. Moreover, the HC exhibited GP at 2734 W, which was better than the other topologies except for TCT, BLTCT and BLHC with decent ML (14.56%) and FF (66.49%), which was comparable to hybrid topologies. From the simulation results from Figures 7-14, the TCT configuration increased the GP to +4.84%, +2.46%, +0.51%, +1.25%, +0.36%, +0.36% and +2.15% when compared to SP, TCT, BL, HC, LD, BLHC, BLTCT and SPTCT, respectively. Here, '+' sign indicates power gain.

Table 7. Assessment parameters of PV array configurations under the UCRS pattern.

Configurations	V_{oc} (V)	I_{sc} (A)	GP Parameters			LP Parameters	No. of LPs	*ML* (%)	*FF* (%)
			V_{mp} (V)	I_{mp} (A)	P_{mp} (W)	$V_{mp}; I_{mp}; P_{mp}$			
SP	190.4	21.64	163.5	16.03	2621	130.7; 18.01; 2354 84.51; 19.65; 1661	2	18.09	63.61
TCT	190.6	21.58	165.7	16.75	2748	121.4; 18.5; 2246 78.28; 20.03; 1568	2	14.13	67.48
BL	190.5	21.64	164.3	16.32	2682	125.8; 18.05; 2334 84.4; 19.68; 1661	2	16.19	65.04
HC	190.1	21.63	164.7	16.6	2734	122.6; 18.39; 2255 80.29; 19.82; 1592	2	14.56	66.49
LD	190.6	21.63	165	16.45	2714	124.8; 18.22; 2275 81.72; 19.6; 1602	2	15.19	65.84
BLHC	190.6	21.63	165.9	16.5	2738	122.2; 18.48; 2259 78.33; 20.02; 1568	2	14.44	66.40
BLTCT	190.6	21.63	165.4	16.55	2738	122.8; 18.34; 2253 79.35; 19.97; 1585	2	14.44	66.40
SPTCT	190.4	21.63	164.5	16.35	2690	123.7; 18.29; 2263 82.71; 19.91; 1647	2	15.94	65.31

6.5. DS Pattern

For this assessment, the solar irradiance of the first diagonal modules was changed as per Figure 5d. The various performance parameters are listed in Table 8 for all array configurations. The topologies such as SP and BL produced one LP, and other topologies produced two LPs. Under the UCRS pattern, the TCT produced LPs at 2192 W; 718.6 W, and GP at 162.8 V; 17.51 A; 2851 W. The ML was equal to 10.90% with FF equal to 71.18%, which was highest among all the array topologies. The hybrid BLHC array configuration exhibited LPs at 755.2 W; 2198 W and GP at 2849 W with 10.97%, ML and 70.87%, FF. The maximum power generation was just 2 W less than the TCT configuration, but it was better than other configurations. The BLTCT exhibited GP at 2833 W, which was better than the other topologies except for TCT and BLHC with an ML equal to 11.47%, and FF equal to 70.50%. The ML and FF of SP, SPTCT, LD and BL topologies were poor, which was almost equal to 25.5%; 57.87%, 20.59%; 61.83%, 16.88%; 64.54% and 16.88%; 64.54%, respectively. From the simulation results from Figures 7–14, the TCT configuration increased the power generation to +19.58%, +19.58%, +1.27%, +7.18%, +17.22%, +0.071%, +0.63% and +1.22% when compared to SP, BL, HC, LD, BLHC, BLTCT and SPTCT, respectively.

Table 8. Assessment parameters of PV array configurations under the DS pattern.

Configurations	V_{oc} (V)	I_{sc} (A)	GP Parameters			LP Parameters	No. of LPs	ML (%)	FF (%)
			V_{mp} (V)	I_{mp} (A)	P_{mp} (W)	$V_{mp}; I_{mp}; P_{mp}$			
SP	190.4	21.63	118.7	20.08	2384	167.9;13.36;2243	1	25.5	57.87
TCT	190.6	21.01	162.8	17.51	2851	117.3;16.2;2192 35.75;19.58;718.6	2	10.90	71.18
BL	190.5	21.64	119.3	19.98	2384	168.3;13.5;2273	1	25.50	57.82
HC	191.3	21.08	162.2	17.35	2815	122.5;18.52;2268 38.11;20.03;763.2	2	12.03	69.79
LD	190.5	21.63	165.9	16.03	2660	121;17.98;2176 80.8;19.83;1602	2	16.88	64.54
BLHC	190.6	21.08	162.8	17.49	2849	119;18.47;2198 37.42;20.18;755.2	2	10.97	70.87
BLTCT	190.6	21.08	162.6	17.42	2833	122;18.34;2237 37.85;20.07;759.9	2	11.47	70.50
SPTCT	190.4	21.58	165.5	15.35	2541	122.7;18.32;2249 82.71;19.91;1647	2	20.59	61.83

6.6. R-I Pattern

For this assessment, the solar irradiance of the random modules was changed as per Figure 5e. The various performance parameters are listed in Table 9 for all array configurations. The topologies such as TCT, BLHC and LD produced two LPs, and other topologies produced three LPs. Under R-I pattern, the TCT produces LPs at 714.7 W; 1926 W and GP at 165.1 V; 14.50 A; 2394 W. The ML was equal to 25.18% with FF equal to 61.59%, which was highest among all the array topologies. The hybrid BLHC configuration exhibited LPs at 731 W; 1910 W, and GP at 2389 W with 25.34%, ML, and 61.30%, FF. The maximum power generation was 5 W less than the TCT configuration and better than other topologies. The BL exhibited GP at 2352 W, which was better than the other topologies except for TCT and BLHC with ML equal to 26.50% and FF equal to 60.30%. From the simulation results from Figures 7–14, the TCT configuration increased the power generation to +9.96%, +1.78%, +7.11%, +9.46%, +0.2%, +3.81% and +4.17% when compared to SP, BL, HC, LD, BLHC, BLTCT and SPTCT, respectively.

Table 9. Assessment parameters of PV array configurations under the R-I pattern.

Configurations	V_{oc} (V)	I_{sc} (A)	GP Parameters			LP Parameters	No. of LPs	*ML* (%)	*FF* (%)
			V_{mp} (V)	I_{mp} (A)	P_{mp} (W)	$V_{mp}; I_{mp}; P_{mp}$			
SP	189.7	21.03	164.1	13.26	2177	125.5; 15.87; 1992 80.17; 16.65; 1335 39.26; 19.53; 767.1	3	31.96	54.54
TCT	189.8	20.48	165.1	14.5	2394	121.3; 15.88; 1926 37.58; 19.02; 714.7	2	25.18	61.59
BL	189.8	20.54	164.4	14.3	2352	126; 15.55; 1959 81.33; 16.71; 1359 38.34; 18.97; 727.3	3	26.50	60.30
HC	189.8	20.54	166.5	13.42	2235	124; 15.76; 1955 80.84; 17.07; 1380 39.22; 19.03; 746.3	3	30.16	57.32
LD	189.7	21.08	163.1	13.41	2187	125.8; 15.95; 2006 39.23; 19.18; 752.5	2	31.66	54.69
BLHC	189.7	20.54	164.6	14.51	2389	120.4; 15.86; 1910 39.28; 18.63; 731	2	25.34	61.30
BLTCT	189.7	21.08	165.4	13.94	2306	122.5; 15.88; 1946 80.66; 16.94; 1367 39.19; 18.66; 731.1	3	27.94	57.66
SPTCT	189.7	21.03	165.5	13.88	2298	122.6; 15.82; 1940 81.76; 16.91; 1383 37.98; 19.14; 727	3	28.19	57.58

6.7. R-II Pattern

For this assessment, the solar irradiance of the random modules was changed as per Figure 5f. The various performance parameters are listed in Table 10 for all array configurations. Except for TCT and BLHC configuration, other topologies such as SP, BL, HC, LD, BLTCT and SPTCT produced three LPs. Under the R-II pattern, the TCT produced LPs at 750.6 W; 1458 W and GP at 167 V; 11.77 A; 1966 W. The ML was equal to 38.56% with FF equal to 48.11%, which was highest among all the array topologies. The BLHC array configuration exhibited LPs at 751.7 W; 1458 W, and GP at 1966 W with 38.56%, ML, and 47.99%, FF. From the simulation results from Figures 7–14, the TCT configuration increased the power generation to +10.01%, +12.72%, +2.66%, +2.39%, 0%, +2.28% and +9.04% when compared to SP, BL, HC, LD, BLHC, BLTCT and SPTCT, respectively.

Table 10. Assessment parameters of PV array configurations under the R-II pattern.

Configura tions	V_{oc} (V)	I_{sc} (A)	GP Parameters			LP Parameters	No. of LPs	ML (%)	FF (%)
			V_{mp} (V)	I_{mp} (A)	P_{mp} (W)	$V_{mp; }I_{mp; }P_{mp}$			
SP	**189.6**	**21.62**	**123.9**	**14.42**	1787	171.6;9.35;1606 79.54;18.331458 38.12;19.7;751.2	3	44.15	43.58
TCT	189.5	21.56	167	11.77	1966	79.13;18.42;1458 38.24;20.01;750.6	2	38.56	48.11
BL	189.4	21.62	125.2	13.93	1744	170.9;9.878;1688 79.68;18.3;1458 37.61;19.99;752.6	3	45.50	42.59
HC	189.5	21.62	168.5	11.37	1915	124.4;12.47;1553 79.48;18.18;1458 37.73;19.94;752.1	3	40.16	46.76
LD	189.5	21.62	167.8	11.44	1920	125.8;12.42;1563 79.71;18.29;1458 37.6;20;752.1	3	40.00	46.85
BLHC	189.5	21.62	166.2	11.83	1966	79.69;18.3;1458 37.42;20.09;751.7	2	38.56	47.99
BLTCT	189.5	21.62	168.2	11.42	1922	125.8;12.44;1565 79.43;18.36;1458 37.17;20.2;750.6	3	39.94	46.88
SPTCT	189.6	21.62	124.6	14.47	1803	171.6;9.37;1608 79.32;18.38;1458 37.34;20.12;751.4	3	43.66	43.98

6.8. RPL and RPG Comparison

Sections 6.1–6.7. discuss the performance parameters of various PV array topologies under different shading patterns. For a better understanding of the readers, this section discussed the comparison of various array topologies based on the RPL and RPG. The comparison table is given in Table 11 and Table 12. Figure 15 shows the maximum power generation of all the topologies under various shading patterns. Figure 16 and Figure 17 show a comparison between various PV array topologies under different shading patterns in terms of RPL and RPG.

Table 11. Relative power loss (RPL) comparison of various array topologies.

Confi gurations	URS (P_{the} = 2880 W)		UCS (P_{the} = 2940 W)		UCRS (P_{the} = 2960 W)		DS (P_{the} = 2920 W)		RS-1 (P_{the} = 2580 W)		RS-2 (P_{the} = 2440 W)	
	P_{mp} (W)	RPL (W)	P_{mp} (W)	RPL (W)	P_{mp} (W)	RPL (W)	P_{mp} (W)	RPL (W)	P_{mp} (W)	RPL (W)	P_{mp} (W)	RPL (W)
SP	2384	496	2740	200	2621	339	2384	536	2177	403	1787	653
TCT	**2384**	**496**	**2859**	**81**	**2748**	**212**	**2851**	**69**	**2394**	**186**	**1966**	**474**
BL	2384	496	2791	149	2682	278	2384	536	2352	228	1744	696
HC	2384	496	2819	121	2734	226	2815	105	2235	345	1915	525
LD	2384	496	2791	149	2714	246	2660	260	2187	393	1920	520
BLHC	**2384**	**496**	**2842**	**98**	**2738**	**222**	**2849**	**71**	**2389**	**191**	**1966**	**474**
BLTCT	2384	496	2841	99	2738	222	2833	87	2306	274	1922	518
SPTCT	2384	496	2825	115	2690	270	2541	379	2298	282	1803	637

Bold values point toward the best performance of PV array configurations.

Table 12. Relative power gained (RPG) comparison of various array topologies.

Config rations	URS		UCS		UCRS		DS		RS-1		RS-2	
	P_{mp} (W)	RPG (%)	P_{mp} (W)	RPG (%)	P_{mp} (W)	RPG (%)	P_{mp} (W)	RPG (%)	P_{mp} (W)	RPG (%)	P_{mp} (W)	RPG (%)
SP	2384	0	2740	0	2621	0	2384	0	2177	0	1787	0
TCT	**2384**	**0**	**2859**	**4.34**	**2748**	**4.85**	**2851**	**19.58**	**2394**	**9.96**	**1966**	**10.01**
BL	2384	0	2791	1.86	2682	2.33	2384	0.00	2352	8.04	1744	−2.41
HC	2384	0	2819	2.88	2734	4.31	2815	18.08	2235	2.66	1915	7.16
LD	2384	0	2791	1.86	2714	3.55	2660	11.58	2187	0.46	1920	7.44
BLHC	**2384**	**0**	**2842**	**3.72**	**2738**	**4.46**	**2849**	**19.51**	**2389**	**9.74**	**1966**	**10.02**
BLTCT	2384	0	2841	3.69	2738	4.46	2833	18.83	2306	5.93	1922	7.55
SPTCT	2384	0	2825	3.10	2690	2.63	2541	6.59	2298	5.56	1803	0.90

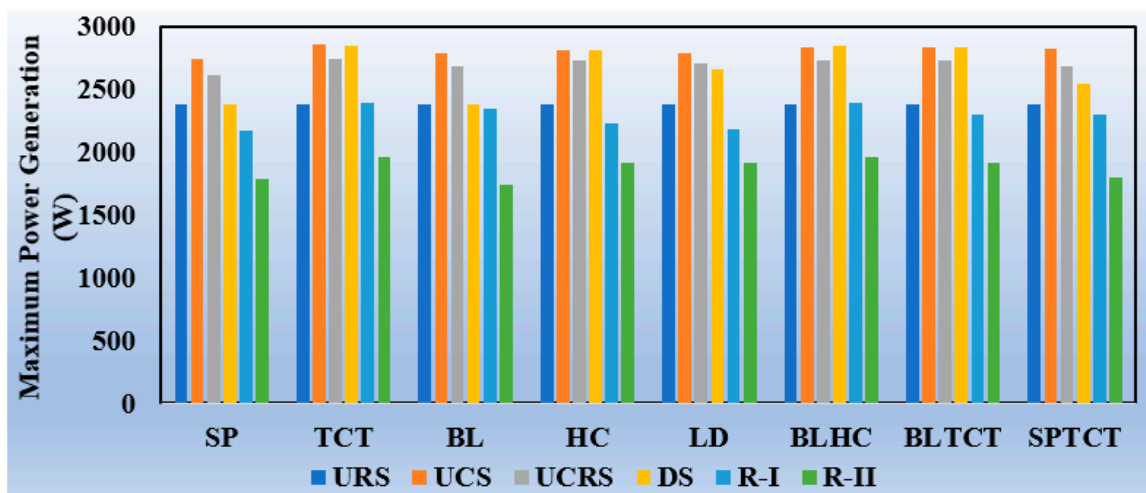Bold values point toward the best performance of PV array configurations.

Figure 15. Maximum output power generation under shading conditions.
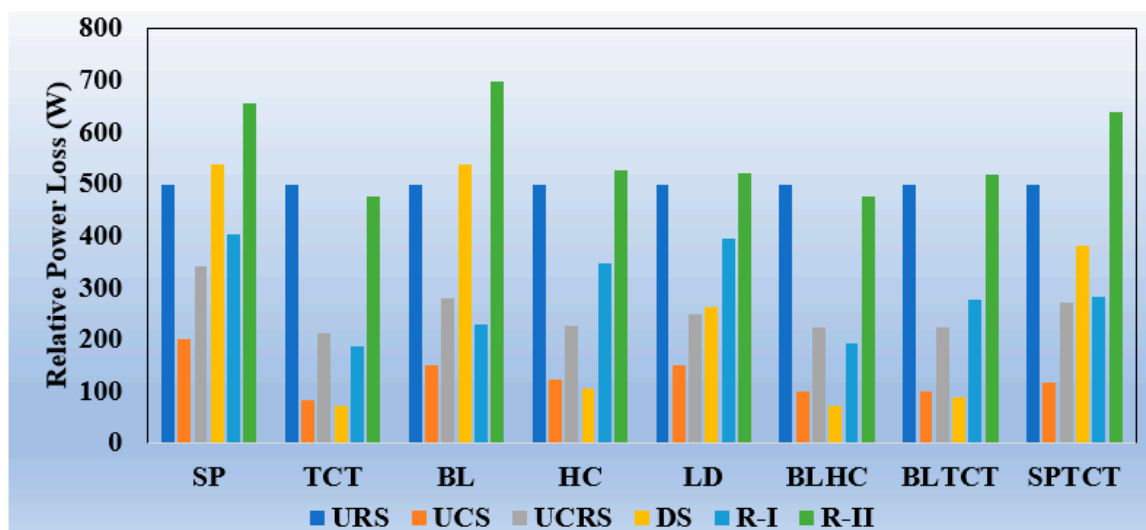

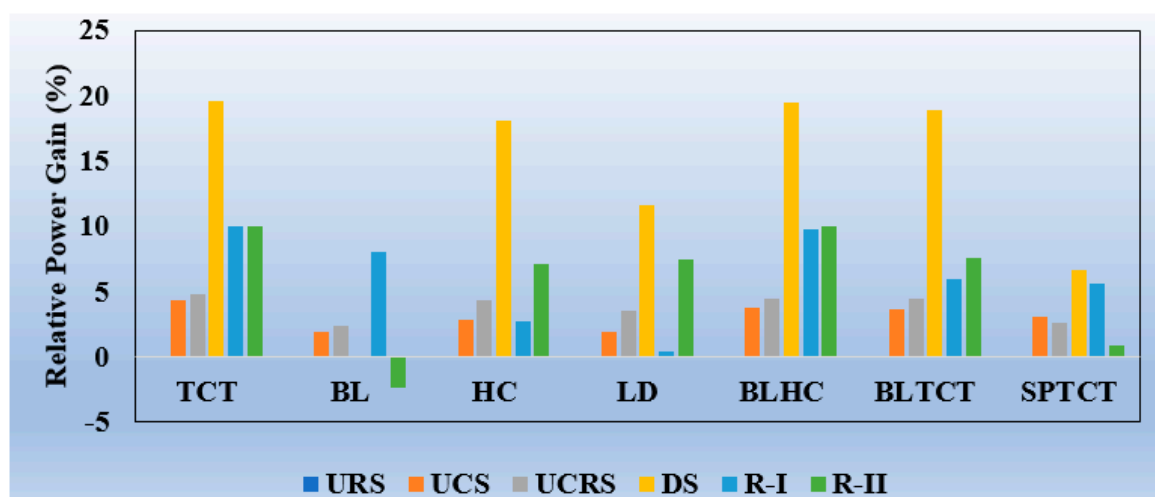**Figure 16.** Comparison between various configurations in terms of RPL.

Figure 17. Comparison between various configurations in terms of RPG.

The results obtained from the simulation results described the relationship between the PV array output power and the type of interconnection within the PV array. From Table 11 and Figure 16, the PV array topologies were ordered in ascending order in terms of RPL as follows: SP > BL > LD > SPTCT > HC > BLTCT > BLHC > TCT and from Table 12 and Figure 17, the PV array topologies were ordered in ascending order in terms of RPG as follows: SP < BL < LD < SPTCT < HC < BLTCT < BLHC < TCT. Besides, the simulation results concluded that the TCT array configuration was superior to other PV array topologies with the least power loss, 14%, and high-power gain, 19.51%. Moreover, the BLHC PV array configuration was performing better than the BL, SP, HC, LD, BLTCT and SPTCT, and the performance was competitive to TCT with less complexity in electrical wiring than the TCT configuration. So, the power loss of the PV system with the BLHC PV array configuration was less than the PV system with the TCT array configuration due to less electrical wiring and hence power loss.

7. Conclusions

This paper assessed the performance of the conventional and the hybrid topologies that affect the maximum power generation of the PV system under different shading patterns. Moreover, this paper discussed the mathematical analysis of the HC PV array topology, which is not covered in previous publications, and the expressions for the voltage and current were derived for UCS and URS patterns. The simulation was carried out to check the effectiveness of all the configurations under static and dynamic shading patterns. The PV array characteristics such as P–V and I–V characteristics were analyzed under various shading patterns, as discussed above. The performance of the array configurations was assessed based on the parameters such as V_{oc}, I_{sc}, GP, LPs, voltage and current of the individual GP and LPs, ML, RPG, RPL and FF. All the topologies were simulated with the bypass diode to maximize the power under PSCs. This paper discussed the reduction of MLs in the PV array using a bypass diode and stringing arrangement approaches. By using both methods, the PV array could generate the maximum output by mitigating the ML significantly. Under various shading patterns, the TCT configuration was superior in producing the maximum output power than the other topologies. However, this paper also reported that the hybrid BLHC topology could perform as similar to TCT, and the performance was comparable to TCT in terms of electrical wiring complexity. From the results, it is noticed that both the BLHC and TCT topology was optimal when the modules were shaded in a single string. If the shading is spread across the strings, then BLHC is optimal topology. If shaded modules are spread across half of the total strings, either SP or TCT or BLHC or HC may be optimal depending on the shading intensity. It is also observed that a greater number of series-connected modules increased the MLs. Based on this criterion, the descending order of the configuration was as follows: TCT, BLHC, BLTCT, HC, SPTCT, LD, BL and SP PV array

configuration. An alternative configuration increased the output power by 1.2%, 1.8%, 3.2%, 3.4%, 3.3%, 3.1% and 2.8% for BL, LD, HC, TCT, BLHC, BLTCT and SPTCT topologies, respectively as compared to the SP configuration. Even though the alterations in PV array configuration seemed to be key to fighting against MLs, the estimation of an additional wiring and frequent maintenance of the PV plant should be addressed to establish the cost-effective alternative array configuration designs. The study on various PV array configurations may be tested and verified in the physical site by considering various shading factors and other experimental factors.

Author Contributions: M.P.K. was originally responsible for conceptualization, methodology, simulation and prepared the original draft of the article. U.S. verified the simulation data, draft writing, and also provided technical guidance. T.S.B. made a formal analysis of the technical write-up, and T.S.B. also collected the technical resources along with the formal editing of the paper. R.M.E. made formal analysis, investigated the simulation data and reviewed the overall content of the paper. R.M.E. and L.M.P. have done an overall review, editing and supervision. All authors have read and agreed to the published version of the manuscript.

Conflicts of Interest: The authors declare no conflict of interest.

Nomenclature

List of Symbols

I_{pv}, $I_{pv,P}$ and I_{ar}	PV cell, PV module and PV array current in A, respectively
I_{photo}	Photocurrent in A
I_0	Diode saturation current in A
q	Electron charge in C
V, V_P, and V_{ar}	PV cell, PV module and PV array voltage in V, respectively
R_{se} and R_p	Series and shunt resistance of the PV cell in Ω, respectively
N_{se} and N_s	Number of series connected PV cells and PV modules, respectively
N_p	Number of parallel connected PV modules
a	Diode ideality factor
k	Boltzmann constant in J/K
T	Cell temperature in K
V_{oc} and I_{sc}	Open circuit voltage in V and short circuit current in A of the PV module/array, respectively
V_{mp} and I_{mp}	Maximum power point voltage in V and current in A of the PV module/array, respectively
P_{mp}	Power at maximum power point in W of the PV module/array
I_{po}	Photocurrent of PV cell at standard solar irradiance, G_o (1000 W/m²)
G	Actual solar irradiance during shading conditions in W/m²
V_n and I_m	Voltage in V and current in A of the respective PV module
V_{out} and I_{out}	Output voltage in V and Output current in A of the PV array, respectively
α	Shading factor
I_n	Current at which the I–V characteristic change its path due to shade in A
P_o	Output power of the PV array in W

$\varDelta P_L$	Mismatching loss in W
P_{the}	Theoretical power generation in W
P_{PSC}	Power generation at certain PSC in W
$P_{mp,i}$	Power at MPP of various PV array topologies in W
$P_{mp,SP}$	Power at MPP of SP PV array configuration in W

List of Abbreviations

PV	Photovoltaic
PSC	Partial shading condition
SP	Series-Parallel
S	Series
HC	Honey-Comb
TCT	Total-Cross-Tied
LD	Ladder
BL	Bridge-Linked
BLHC	Bridge-Linked Honey-Comb
BLTCT	Bridge-Linked Total-Cross-Tied
SPTCT	Series-Parallel Total-Cross-Tied
GP	Global peak
LP	Local peak
FF	Fill factor
ML	Mismatching loss
MPP	Maximum power point
MPPT	Maximum power point tracking
URS	Uneven row shading
UCS	Uneven column shading
UCRS	Uneven corner shading
DS	Diagonal shading
R-I	Random shading-I
R-II	Random shading-II
RPL	Relative power loss
RPG	Relative power generation

References

1. Elavarasan, R.M. Comprehensive review on India's growth in renewable energy technologies in comparison with other prominent renewable energy-based countries. *J. Sol. Energy Eng.* **2020**, *142*, 030801.
2. Elavarasan, R.M.; Shafiullah, G.M.; Manoj Kumar, N.; Padmanaban, S. A state-of-the-art review on the drive of renewables in Gujarat, state of India: Present situation, barriers and future initiatives. *Energies* **2020**, *13*, 40.
3. Elavarasan, R.M.; Shafiullah, G.M.; Padmanaban, S.; Manoj Kumar, N.; Annapurna, A.; Ajayragavan Manavalanagar, V.; Mihet-Popa, L.; Holm-Nielsen, J.B. A comprehensive review on renewable energy development, challenges, and policies of leading Indian states with an international perspective. *IEEE Access* **2020**, *8*, 74432–74457.
4. El-Khozondar, H.J.; El-Khozondar, R.J.; Matter, K. A review study of photovoltaic array maximum power tracking algorithms. *Renew. Wind Water Sol.* **2016**, *3*, 3.

5.　Mohapatra, A.; Nayak, B.; Das, P.; Barada Mohanty, K. A review on MPPT techniques of PV system under partial shading condition. *Renew. Sustain. Energy Rev.* **2017**, *80*, 854–867.

6.　Elavarasan, R.M. The motivation for renewable energy and its comparison with other energy sources: A review. *Eur. J. Sustain. Dev. Res.* **2019**, *3*, em0076.

7.　Bhatnagar, P.; Nema, R.K. Maximum power point tracking control techniques: State-of-the-art in photovoltaic applications. *Renew. Sustain. Energy Rev.* **2013**, *23*, 224–241.

8.　Bana, S.; Saini, R.P. Experimental investigation on power output of different photovoltaic array configurations under uniform and partial shading scenarios. *Energy* **2017**, *127*, 438–453.

9.　Belhachat, F.; Larbes, C. Modeling, analysis and comparison of solar photovoltaic array configurations under partial shading conditions. *Solar Energy* **2015**, *120*, 399–418.

10.　Premkumar, M.; Karthick, K.; Sowmya, R. A comparative study and analysis on conventional solar PV based DC-DC converters and mppt techniques. *Ind. J. Electr. Eng. Comput. Sci.* **2018**, *11*, 831–838.

11.　Premkumar, M.; Sumithira, T.R. Design and implementation of new topology for non-isolated dc-dc microconverter with effective clamping circuit. *J. Circuits Syst. Comput.* **2019**, *28*, 1950082.

12.　Premkumar, M.; Sumithira, T.R. Humpback whale assisted hybrid maximum power point tracking algorithm for partially shaded solar photovoltaic systems. *J. Power Electron.* **2018**, *18*, 1805–1818.

13.　Rezk, H.; Eltamaly, A. A comprehensive comparison of different MPPT techniques for photovoltaic systems. *Sol. Energy* **2015**, *112*, 1–11.

14.　Islam, H.; Mekhilef, S.; Shah, N.B.M.; Soon, T.K.; Seyedmahmousian, M.; Horan, B.; Stojcevsk, A. Performance evaluation of maximum power point tracking approaches and photovoltaic systems. *Energy* **2018**, *11*, 365.

15.　Sudhakar Babu, T.; Sangeetha, K.; Rajasekar, N. Voltage band based improved particle swarm optimization technique for maximum power point tracking in solar photovoltaic system. *J. Renew. Sustain. Energy* **2016**, *8*, 013106.

16.　Azharuddin, S.; Mohammed, M.; Vysakh, M.; Harshal Vilas, T.; Nishant, B.; Sudhakar Babu, T.; Muralidhar, K.; Don, P.; Basil, J.; Balasubramanian, K.; et al. A near accurate solar PV emulator using dSPACE controller for real-time control. *Energy Proc.* **2014**, *61*, 2640–2648.

17.　Sangeetha, K.; Sudhakar Babu, T.; Rajasekar, N. Fireworks algorithm-based maximum power point tracking for uniform irradiation as well as under partial shading condition. In *Artificial Intelligence and Evolutionary Computations in Engineering Systems*; Dash, S.S., Chandra Babu Naidu, P., Bayindir, R., Das, S., Eds.; Springer: Berlin/Heidelberg, Germany, 2016; pp. 79–88.

18.　Yousri, D.; Sudhakar Babu, T.; Allam, D.; Ramachandaramurthy, V.K.; Magdy, B. Etiba. A novel chaotic flower pollination algorithm for global maximum power point tracking for photovoltaic system under partial shading conditions. *IEEE Access* **2019**, *7*, 121432–121445.

19.　Dalia, Y.; Sudhakar Babu, T.; Allam, D.; Ramachandaramurthy, V.K.; Beshr, E.; Eteiba, M. Fractional chaos maps with flower pollination algorithm for partial shading mitigation of photovoltaic systems. *Energies* **2019**, *12*, 3548.

20.　Premkumar, M.; Mohamed Ibrahim, A.; Mohan Kumar, R.; Sowmya, R. Analysis and simulation of bio-inspired intelligent salp swarm MPPT method for the PV systems under partial shaded conditions. *Inter. J. Comput. Digit. Syst.* **2019**, *8*, 489–496.

21.　Manganiello, P.; Ballato, M.; Vitelli, M. A survey on mismatching and aging of PV modules: The closed-loop. *IEEE Trans. Ind. Electron.* **2015**, *62*, 7276–7286.

22.　Gow, J.A. Development of a model for photovoltaic arrays suitable for use in simulation studies of solar energy conversion systems. In Proceedings of the 6th International Conference on Power Electronics and Variable Speed Drives, Nottingham, UK, 23–25 September 1996; pp. 69–74.

23.　Di Vincenzo, M.C.; Infield, D. Detailed PV array model for non-uniform irradiance and its validation against experimental data. *Sol. Energy* **2013**, *97*, 314–331.

24.　Yousri, D.; Dalia, A.; Eteiba, M.B. Optimal photovoltaic array reconfiguration for alleviating the partial shading influence based on a modified harris hawks optimizer. *Ener. Conv. Mana.* **2020**, *206*, 112470.

25.　Bingo, O.; Ozkaya, B. Analysis and comparison of different PV array configurations under partial shading conditions. *Sol. Energy* **2018**, *160*, 336–343.

26.　Picault, D.; Raison, B.; Bacha, S.; Aguilera, J.; De La Casa, J. Changing photovoltaic array interconnections to reduce mismatch losses: A case study. In Proceedings of the 2010 9th International Conference on Environment and Electrical Engineering, Prague, Czech Republic, 16–19 May 2010; pp. 37–40.

27. Maki, A.; Valkealahti, S. Power losses in long string and parallel-connected short strings of series-connected silicon-based photovoltaic modules due to partial shading conditions. *IEEE Trans. Energy Conv.* **2012**, *27*, 173–183.

28. Bizon, N. Global extremum seeking control of the power generated by a photovoltaic array under partially shaded conditions. *Energy Conv. Manag.* **2015**, *109*, 71–85.

29. Niazi, K.A.K.; Yang, Y.; Nasir, M.; Sera, D. Evaluation of Interconnection Configuration Schemes for PV Modules with Switched-Inductor Converters under Partial Shading Conditions. *Energies* **2019**, *12*, 2802.

30. Bidram, A.D.; Balog, S. Control and circuit techniques to mitigate partial shading effects in Photovoltaic arrays. *IEEE J. Photovolt.* **2012**, *2*, 532–546.

31. Nnamchi, S.N.; Oko, C.O.C.; Kamen, F.L.; Sanya, O.D. Mathematical analysis of interconnected photovoltaic arrays under different shading conditions. *Cogent Eng.* **2018**, *5*, 1507442.

32. Mohammadnejad, S.; Khalafi, A.; Morteza Ahmadi, S. Mathematical analysis of total-cross-tied photovoltaic array under partial shading condition and its comparison with other configurations. *Sol. Energy* **2016**, *133*, 501–511.

33. Wang, Y.J.; Hsu, P. Analysis of partially shaded PV modules using piecewise linear parallel branches model. *World Acad. Sci. Eng. Tech.* **2009**, *60*, 783–789.

34. Teo, J.C.; Rodney, H.G. Tan.; Mok, V.H.; Ramachandaramurthy, V.K.; Kwang Tan, C. Impact of partial shading on the P–V characteristics and the maximum power of a photovoltaic string. *Energies* **2018**, *11*, 1860.

35. Wang, Y.J.; Hsu, P.C. An investigation on partial shading of PV modules with different connection configurations of PV cells. *Energy* **2011**, *36*, 3069–3078.

36. Yadav, A.S.; Pachauri, R.K.; Chauhan, Y.K. Comprehensive investigation of PV arrays with puzzle shade dispersion for improved performance. *Sol. Energy* **2016**, *129*, 256–285.

37. Yadav, A.S.; Pachauri, R.K.; Chauhan, Y.K.; Choudhury, S.; Singh, R. Performance enhancement of partially shaded PV array using novel shade dispersion effect on magic-square puzzle configuration. *Sol. Energy* **2017**, *144*, 780–797.

38. Ishaque, K.; Salam, Z.; Syafaruddin, A. A comprehensive MATLAB Simulink PV system simulator with partial shading capability based on two diode model. *Sol. Energy* **2011**, *85*, 2217–2222.

39. Qi, J.; Zhang, Y.; Chen, Y. Modeling and maximum power point tracking (MPPT) method for PV array under partial shade conditions. *Renew. Energy* **2014**, *66*, 337–345.

40. Karatepe, E.; Boztepe, M.; Colak, M. Development of a suitable model for characteristics photovoltaic arrays with shaded solar cells. *Sol. Energy* **2007**, *81*, 977–992.

41. Malathy, S.; Ramaprabha, R. Comparative analysis on the role of array size and configuration on energy yield of photovoltaic systems under shaded conditions. *Renew. Sustain. Energy Rev.* **2015**, *49*, 672–679.

42. Pareek, S.; Dahiya, R. Output power maximization of partially shaded 4*4 PV field by altering its topology. *Energy Proc.* **2014**, *54*, 116–126.

43. Patel, H.; Agarwal, V. MATLAB-based modeling to study the effects of partial shading on PV array characteristics. *IEEE Trans. Energy Conv.* **2008**, *23*, 302–310.

44. Kaushika, N.D.; Gautam, N.K. Energy yield simulations of interconnected solar PV arrays. *IEEE Trans. Energy Conv.* **2003**, *18*, 127–134.

45. Ramaprabha, R.; Mathur, B.L. A comprehensive review and analysis of solar photovoltaic array configurations under partial shaded conditions. *Int. J. Photoenergy* **2012**, *2012*, 120214.

46. Prince Winston, D.; Kumaravel, S.; Praveen Kumar, B.; Devakirubakaran, S. Performance improvement of solar PV array topologies during various partial shading conditions. *Sol. Energy* **2020**, *196*, 228–242.

47. Yadav, A.S.; Yadav. V.K.; Choudhary, S. Power enhancement from solar pv array topologies under partial shading condition. In Proceedings of the International Conference on Power Energy, Environment and Intelligent Control, Greater Noida, India, 13–14 April 2018; pp. 379–383.

48. Kumar, K.; Vikas, G. A Comprehensive review on grid-tied solar photovoltaic system. *J. Green Eng.* **2017**, *7*, 213–254.

49. Sharip, M.R.M.; Haidar, A.M.A.; Jimel, A.C. Optimum configuration of solar PV topologies for dc microgrid connected to the longhouse communities in Sarawak, Malaysia. *Int. J. Photoenergy.* **2019**, *2019*, 2657265.

50. Agrawal, N.; Avinashi, K. Power loss mitigation in partially shaded solar PV array through different interconnection topologies. *AIP Conf. Proc.* **2019**, *2136*, 040012.

51. Amer Chaaban, M.; El Chaar, L.; Alahmad, M. An adaptive photovoltaic topology to overcome shading effect in PV systems. *Int. J. Photoenergy.* **2015**, *2015*, 294872.

52. Gonzalez Montoya, D.; David Bastidas-Rodriguez, J.; Adriana Trejos-Grisales, L.; Andres Ramos-Paja, C.; Petrone, G.; Spagnuolo, G. A procedure for modeling photovoltaic arrays under any configuration and shading conditions. *Energies* **2018**, *11*, 767.

53. Seyedmahmoudian, M.; Mekhilef, S.; Rahmani, R.; Yusof, R.; Renani, E.T. Analytical modeling of partially shaded photovoltaic systems. *Energies* **2013**, *6*, 128–144.

54. Petrone, G.; Ramos-Paja, C.A. Modeling of photovoltaic fields in mismatched conditions for energy yield evaluations. *Electr. Power Syst. Res.* **2011**, *81*, 1003–1013.

55. Kajihara, K.; Harakawa, T. Model of photovoltaic cell circuits under partial shading. In Proceedings of the IEEE International Conference on Industrial Technology, Taipei, China, 14–17 December 2005; pp. 866–870.

56. Villalva, M.G.; Gazoli, J.R.; Filho, E.R. Comprehensive approach to modelling and simulation of photovoltaic arrays. *IEEE Trans. Power Electron.* **2009**, *24*, 1198–1208.

57. Gao, L.; Dougal, R.A.; Liu, S.; Iotova, A.P. Parallel-connected solar PV system to address partial and rapidly fluctuating shadow conditions. *IEEE Trans. Ind. Electron.* **2009**, *56*, 1548–1556.

58. Babu, T.S.; Yousri, D.; Balasubramanium, K. Photovoltaic array reconfiguration system for maximizing the harvested power using population-based algorithms. *IEEE Access.* **2020**, 13, 1-15, 10.1109/ACCESS.2020.3000988.

59. Rani, B. Enhanced power generation from PV array under partial shading conditions by shade dispersion using Su-Do-Ku configuration. *IEEE Trans. Sustain. Energy* **2013**, *4*, 594–601.

60. Horoufiany, M.; Ghandehari, R. Optimization of the Sudoku based reconfiguration technique for PV arrays power enhancement under mutual shading conditions. *Sol. Energy* **2018**, *159*, 1037–1046.

61. Romano, P.; Candela, R.; Cardinale, M.; Li Vigni, V.; Musso, D.; Sanseverino, E.R. Optimization of photovoltaic energy production through an efficient switching matrix. *J. Sustain. Dev. Energy Water Environ. Syst.* **2013**, *1*, 227–236.

62. Shubhankar Niranjan, D.; Bhaskar Dhale, S.; Shekar Mukherjee, J.; Sudhakar Babu, T.; Rajasekar, N. Solar PV array reconfiguration under partial shading conditions for maximum power extraction using genetic algorithm. *Renew. Sustain. Energy Rev.* **2015**, *43*, 102–110.

63. Sudhakar Babu, T.; Prasanth Ram, J.; Dragičević, T.; Miyatake, M.; Blaabjerg, F.; Rajasekar, N. Particle swarm optimization based solar PV array reconfiguration of the maximum power extraction under partial shading conditions. *IEEE Trans. Sustain. Energy* **2017**, *9*, 74–85.

64. Raju Pendem, S.; Mikkili, S. Modeling, simulation, and performance analysis of PV array configurations (Series, Series-Parallel, Bridge-Linked, and Honey-Comb) to harvest maximum power under various Partial Shading Conditions. *Int. J. Green Energy* **2018**, *15*, 795–812.

65. Topić, D.; Knežević, G.; Fekete, K. The mathematical model for finding an optimal PV system configuration for the given installation area providing a maximal lifetime profit. *Sol. Energy* **2017**, *144*, 750–757.

66. Sai Krishna, G.; Moger, T. Improved SuDoKu reconfiguration technique for total-cross-tied PV array to enhance maximum power under partial shading conditions. *Renew. Sustain. Energy Rev.* **2019**, *109*, 333–348.

67. Velasco-Quesada, G.; Guinjoan-Gispert, F.; Pique-Lopez, R.; Roman Lumbreras, M.; Conesa-Roca, A. Electrical PV array reconfiguration strategy for energy extraction improvement in grid-connected PV systems. *IEEE Trans. Ind. Electron.* **2009**, *56*, 4319–4331.

68. Nguyen, D.; Lehman, B. A reconfigurable solar photovoltaic array under shadow conditions. In Proceedings of the 23rd Annual IEEE Applied Power Electronics Conference and Exposition, Austin, TX, USA, 24–28 February 2008; pp. 980–986.

69. Rakesh, N.; Madhavaram, T.V. Performance enhancement of partially shaded solar PV array using novel shade dispersion technique. *Front. Energy* **2016**, *10*, 227–239.

70. Patnaik, B.; Sharma, P.; Trimurthulu, E.; Duttagupta, S.P.; Agarwal, V. Reconfiguration strategy for optimization of solar photovoltaic array under non-uniform illumination conditions. In Proceedings of the 37th IEEE Photovoltaic Specialists Conference, Seattle, Washington, USA, 2011**,** pp. 1859–1864.

71. Sagar, G.; Pathak, D.; Gaur, P.; Jain, V. A Su Do Ku puzzle-based shade dispersion for maximum power enhancement of partially shaded hybrid bridge-link-total-cross-tied PV array, *Sol. Energy* **2020**, *204*, 161–180.

72. Pareek, S.; Dahiya, R. Enhanced power generation of partial shaded photovoltaic fields by forecasting the interconnection of modules. *Energy* **2016**, *95*, 561–572.

73. Premkumar, M.; Dhanasekar, N.; Dhivakar, R.; Arunkumar, P. Comparison of MPPT algorithms for PV system-based DC-DC converter. *Adv. Nat. Appl. Sci.* **2016**, *17*, 212–221.

74. Kandemir, E.; Cetin, N.S.; Borekei, S. A comprehensive overview of maximum power extraction methods for PV systems. *Renew. Sustain. Energy Rev.* **2017**, *78*, 93–112.

75. Elavarasan, R.M.; Ghosh, A.; K.; Mallick, T.; Krishnamurthy, A.; Saravanan, M. Investigations on performance enhancement measures of the bidirectional converter in PV–wind interconnected microgrid system. *Energies* **2019**, *12*, 2672.

76. Premkumar, M.; Sumithira, T.R. Design and implementation of new topology for solar pv based transformerless forward microinverter. *J. Electr. Eng. Tech.* **2019**, *14*, 145–155.

77. Alshareef, M.; Lin, Z.; Ma, M.; Cao, W. Accelerated particle swarm optimization for photovoltaic maximum power point tracking under partial shading conditions. *Energies* **2019**, *12*, 623.

78. Premkumar, M.; Sowmya, R. Certain study on mppt algorithms to track the global MPP under partial shading on solar PV module/array. *Int. J. Comput. Digit. Syst.* **2019**, *8*, 405–416.

79. Pendem, S.R.; Mikkili, S. Modelling and performance assessment of PV array topologies under partial shading conditions to mitigate the mismatching power losses. *Sol. Energy* **2018**, *160*, 303–321.

80. Chan, D.S.H.; Phang, J.C.H. Analytical methods for the extraction of solar-cell single-and double-diode model parameters from I–V characteristics. *IEEE Trans. Electron. Dev.* **1987**, *34*, 286–293.

81. Masters, G.M. *Renewable and Efficient Electric Power Systems*, 1st ed.; John Wiley & Sons: New Jersey, NJ, USA, 2004; pp. 154–195.

82. Desoto, W.; Beckman, W.; Klein, S. Improvement and validation of a model for photovoltaic array performance. *Sol. Energy* **2006**, *80*, 78–88.

83. Jain, K.; Kapoor, A. Exact analytical solutions of the parameters of real solar cells using Lambert W-function. *Sol. Energy Mater. Sol. Cells* **2004**, *81*, 269–277.

84. Lindholm, F.A.; Fossum, J.G.; Burgess, E.L. Application of the superposition principle to solar-cell analysis. *IEEE Trans. Electron Devices* **1979**, *26*, 165–171.

85. Mihet-Popa, L.; Koch-Ciobotaru, C.; Isleifsson, F.; Bindner, H. Development of tools for simulation systems in a distribution network and validated by measurements. In Proceedings of the 13th International Conference on Optimization of Electrical and Electronic Equipment, Brasov, Romania, 24–26 May 2012; pp. 1022–1031.

86. Koch-Ciobotaru, C.; Mihet-Popa, L.; Isleifsson, F.; Bindner, H. Simulation model developed for a small-scale PV-system in a distribution network. In Proceedings of the 7th International Symposium on Applied Computational Intelligence and Informatics, Timisoara, Romania, 24–26 May 2012; pp. 257–261.

87. Ackermann, T.; Cherevatskiy, S.; Brown, T.; Eriksson, R.; Samadi, A.; Ghandhari, M.; Söder, L.; Lindenberger, D.; Jägemann, C.; Hagspiel, S.; et al. Smart Modeling of Optimal Integration of High Penetration of PV-SMOOTH PV. Available online: http://smooth-pv.info/doc/SmoothPV_Final_Report_Part1.pdf. (accessed on 20 May 2020).

88. King, D.; Dudley, J.; Boyson, W. *PVSIM: A Simulation Program for Photovoltaic Cells, Modules, and Arrays*; Sandia National Labs.: Washington, DC, USA, 1996; pp. 1295–1297.

89. Silvestre, A.B.; Chouder, A. Study of bypass diodes configuration on PV modules. *Appl. Energy* **2009**, *86*, 1632–1640.

90. Hui, L.; Yunmei, C.; Xiangwei, L. Study of bypass diodes configuration on PV modules with partial shaded. In Proceedings of the Chinese Control and Decision Conference, Nanchang, China, 12 September 2019; pp. 511–515.

91. Wei, H.; Liu, F.; Ji, J.; Zhang, S.; Chen, H. Safety analysis of solar module under partial shading. *Int. J. Photoenergy* **2015**, *2015*, 907282.

92. Priyadarshi, N.; Padmanaban, S.; Ionel, D.M.; Mihet-Popa, L.; Azam, F. Hybrid PV-Wind, Micro-Grid development using quasi-Z-source inverter modeling and control-Experimental investigation. *Energies* **2018**, *11*, 2277.